UNIVERSITY OF OKLAHOMA

GRADUATE COLLEGE

STOCHASTIC DETERMINATION OF FORMATION PARTING PRESSURE FOR WATER INJECTION WELL

A THESIS

SUBMITTED TO THE GRADUATE FACULTY

in partial fulfillment of the requirements for the

Degree of

MASTER OF SCIENCE

By

ZHIYI JING
Norman, Oklahoma
2017

STOCHASTIC DETERMINATION OF FORMATION PARTING PRESSURE FOR WATER INJECTION WELL

A THESIS APPROVED FOR THE
MEWBOURNE SCHOOL OF PETROLEUM AND GEOLOGICAL ENGINEERING

BY

_____
Dr. Xingru Wu, Chair

_____
Dr. Catalin Teodoriu

_____
Dr. Bor-Jier (Ben) Shiau

To mom and dad,

Thank you for everything.

Acknowledgements

I would first like to thank my thesis advisor Dr. Xingru Wu for his consistent support, Patience and guidance throughout my project. As my teacher and mentor, he has taught me more than I could ever give him credit for here. He has shown me, by his example, what a good engineer (and person) should be. This work would not have been possible without his helpful supervision.

I would also like to thank Dr. Catalin Teodoriu and Dr. Ben Shiau for being on my committee, for their time and consideration.

Finally, I must express my very profound gratitude to my parents for providing me with unfailing support and continuous encouragement throughout my years of study and through the process of researching and writing this thesis. Thank you to Rui Zhang, for all his love and company. This accomplishment would not have been possible without them. Thank you.

Table of Contents

List of Tables

List of Figures

Abstract

Water injection is arguably the most widely used technology in maintaining reservoir pressure and enhanced oil recovery. However, the water injectivity always declines as water injection process continuing due to the injection water quality and changes in formation condition. When the injection pressure is above the formation parting pressure, the formation will be fractured, whether inadvertently or purposely. The parting pressure for a depleted reservoir is affected by many parameters including reservoir pore pressure, injection fluid temperature, and rock geomechanics, etc.

In this study, a stochastic modeling is used to determine the parting pressure for water injection. The reason of using Monte Carlo simulation is because petrophysical parameters in the subsurface environment are of a high level of uncertainty, and operator usually knows the range of them to a certain level, but does not know them accurately with high precision. Therefore, Monte Carlo simulation can take the possible distribution into consideration and give the range of possible parting pressure and possibility of occurrence.

Once the formation parting pressure is determined, the operation profile between the injection rate and injection pressure can be established. This project proposes a procedure to determine the injection profile by considering the dynamic well injectivity and injection pressure. The determined profile can be used in injection operation and reservoir management.

The proposed models and procedure are applied in a case study for a water injection well in a producing asset in Gulf of Mexico (GoM). The comparison results showed that the

determined parting pressure matches the field measurements very well and thus the determined injection profile can be used as injection guideline to injecting water through formation matrix or purposely fracturing the matrix.

The work is practically important and scientifically challenging. Operator can use the program to operate water injection wells together with other surveillance tools to well manage the asset. Additionally, the formation parting pressure during water injection is affected by many parameters inherently and many of them have high level of uncertainties. Therefore, the project also proposes some future work to extend the scope of the work.

Chapter 1: Introduction

Water injection is arguable the most often used Enhanced Oil Recovery (EOR) technology. Field practices show that the injectivity of water injection well usually get smaller when a large quantity of water is injected, which results in requiring higher injection pressure in order to keep the same injection rate for reservoir management purpose. Injection induced fracturing could occur in waterflooding when the injection pressure is above the formation parting pressure. However, sometimes the fracturing can occur inadvertently, which could cause many undesirable effects such as matrix bypass event and short-circuit water injection and offset production well. Therefore, a thorough understanding of the formation parting pressure during water injection is critical for reservoir management.

The problem being addressed in this report is to quantitatively determine the formation parting pressure under multiple influencing factors for a water injection well and examine the relative importance of them through sensitivity study. Because subsurface variables have inherent uncertainties in their measurements and interpretations, Monte Carlo simulation is used to stochastically study the range of and possibility of the determined parting pressure. Also, a field example from Gulf of Mexico (GoM) is used as a case study and the calculated results are verified against the downhole gauge measurement.

The outline of the project is as follows. Chapter one is the introduction which states the problem to be solved. Chapter two is literature survey which shows the related research that had been done on this topic. Chapter three is the methodology which presents the

calculation procedure. Chapter four is validation using a Gulf of Mexico field example, and chapter five gives conclusions and observations as well as future works for this study.

Chapter 2: Determining Fracturing Pressure for an Injection Well

Injection-induced fracturing widely occurs in waterflooding process. It has been widely discussed in previous literature by both analytical models and numerical simulation approaches. Research methods have evolved from early simple analytical modeling to recent flow performance and geomechanics coupled numerical simulation which allows more realistic description of problems than analytical and has a broadly applicable range.

Hagoort et al. (1980) provided a semi-analytical model for predicting the fracture propagation induced by water injection during a water flooding. However, thermally induced stress change was ignored in the model. Perkins and Gonzalez (1985) presented a three-region model by coupling the flow performance with fracture mechanics, which has been a base model for the later study on waterflooding induced fracture (Saripalli et al., 1999; Suri et al., 2009; Rahman and Khaksar, 2012). Suri et al. (2010) studied reservoir pressure transient model for fractured injector based on Gringarten's work (1974). The analytical model assumes 1-D fracture growth with an infinite conductivity and ignores width of fracture. Reservoir geomechanical properties variation due to injection cannot be simultaneously updated in this model. In other words, the fracture mechanics and reservoir flow dynamics are decoupled, which implies using these model for a quantitative prediction of fracture growth could be problematic.

The fracture model used in this study was based on Perkins and Gonzalez model and Koning's model. The details of the model and calculation procedure will be discussed in Chapter 2 and Chapter 3.

2.1 Factors Influencing Formation Parting Pressure

2.1.1 In-situ Stress

Underground formations are confined and under stresses. There are three principal earth stresses oriented at right angles to one another: vertical stress, maximum horizontal stress and minimum horizontal stress as shown in **Figure 2-1**. The magnitude and direction of these principal stresses control the pressure required to create and propagate a fracture, the shape and vertical extent of the fracture as well as the direction of the fracture. In principle, a fracture propagates parallel to the greatest principal stress and perpendicular to the least principal stress. That is, for example, if the maximum principal compressive stress is the overburden stress, then vertical fracture paralleling to the maximum horizontal stress is expected when the fracturing pressure exceeds the minimum horizontal stress.

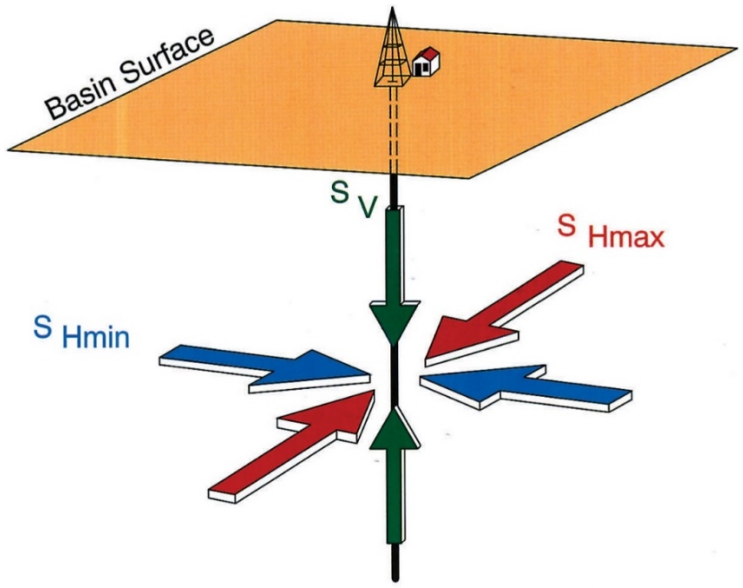

Figure 2-1 In-situ stress in in the subsurface environment. Adapted from http://ags.aer.ca/publications/chapter-29-in-situ-stress. Accessed on July 23, 2017.

The three principal stresses are calculated as follows. For a formation at depth H, the absolute vertical stress, σ_v , is given by

$$\sigma_v = g\int_0^H \rho_f dH \qquad \text{Eqn. 2-1}$$

where ρ_f is the density of the formations overlaying the target reservoir. If the density is constant, the equation above becomes

$$\sigma_v = \frac{\rho H}{144} \qquad \text{Eqn. 2-2}$$

where an average formation density is used in $\mathrm{lb/ft^3}$ and the depth is in ft. For most sandstones, $\rho = 165\ \mathrm{lb/ft^3}$.

In a case of a porous medium, the weight of the overburden is carried by both the rock fabrics and the fluid within the pore space. The corresponding effective vertical stress is defined by

$$\sigma'_v = \sigma_v - \alpha p \qquad \text{Eqn. 2-3}$$

Where,

α: Biot's poroelastic constant

p: pore pressure

For many hydrocarbon reservoirs the Biot's poroelastic constant is approximately equal to 0.7. (Economides, Hill, Ehlig-Economides, & Zhu, 2012).

The effective horizontal stress σ_H' can be translated from vertical stress through the Poisson relationship:

$$\sigma'_H = \frac{\nu}{1-\nu}\sigma_v' \qquad \text{Eqn. 2-4}$$

where ν is the Poisson ratio, and for sandstones it is approximately equal to 0.25. (Economides et al., 2012)

The absolute horizontal stress, σ_H, can be determined as follows:

$$\sigma_H = \sigma'_H + \alpha p \qquad \text{Eqn. 2-5}$$

As the result of tectonic stresses, the horizontal stress is not the same in all directions in the horizontal plane. Therefore, there is a minimum horizontal stress and a maximum horizontal stress:

$$\sigma_{H,max} = \sigma'_{H,min} + \sigma_{tect} \qquad \text{Eqn. 2-6}$$

Where σ_{tect} refers to tectonic stress.

2.1.2 Tectonic Stresses

The tectonic stress is caused by geotectonic movement and is the lateral forces from formation as shown in **Figure 2-2**, which is similar to the crustal movement. Generally speaking, in shallow depths, the tectonic forces have a significant effect on the horizontal stress and lead to a stress type of $\sigma_H > \sigma_v > \sigma_h$ and to a stress type of $\sigma_H > \sigma_h > \sigma_v$ in the intense tectonic zone. For greater depths, the impact of tectonics weakens, and the vertical stress increases and gradually changes the stress type to $\sigma_v > \sigma_H > \sigma_h$ (An & Cheng, 2014). In tectonically active areas, the effects of tectonic activity must be included in the analyses of the total stresses. The pressure required to fracture the formation is intimately connected with the stresses prevailing in the earth's crust and the mechanical

strength of the rock itself (Morgenstern, 1962). Therefore, it may be possible to predict the pressures required to induce fracture if the strength of the rock can be measured and the local stresses inferred.

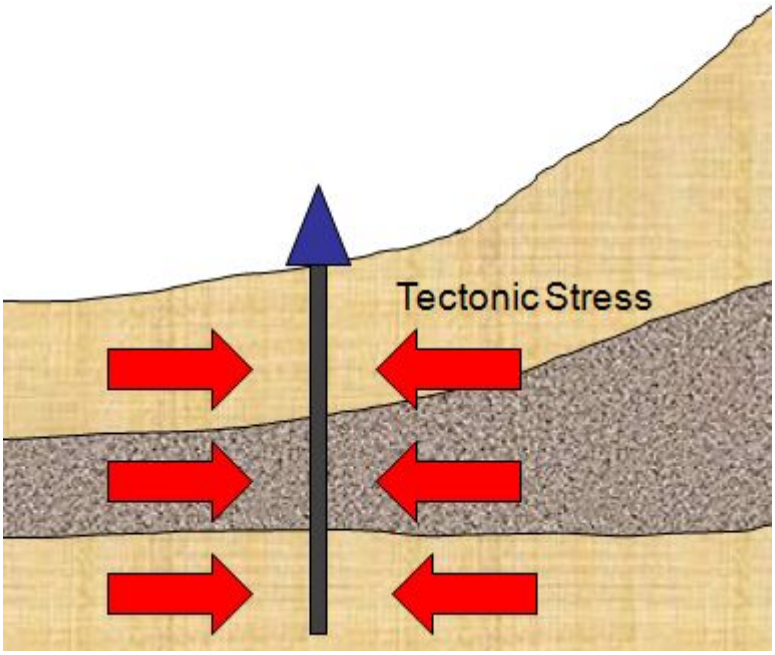

Figure 2-2 Illustration of Tectonic stress for a well in subsurface environment, excepted from https://courses.lumenlearning.com/geophysical/chapter/causes-and-types-of-tectonic-stress/. Accessed on July 23, 2017.

2.1.3 Poroelastic Stress

Pore pressure change due to injection may induce poroelastic stress in the formation rock. Poroelastic stress at wellbore wall (Biot, 1957) is defined as

$$\Delta\sigma^P = \alpha_p \Delta P \qquad \text{Eqn. 2-7}$$

with the effect of geometry of thermal front,

$$\Delta\sigma^P = S_f \frac{\alpha_p E \Delta P}{1-\nu} \qquad \text{Eqn. 2-8}$$

where,

ΔP: the difference between fluid pressure and pore, psi

E: Young's modulus, psi

ν: Poisson ratio

α_p: the coefficient of pore pressure expansion defined as

$$\alpha_p = \alpha \frac{1 - 2\nu}{1 - \nu} \qquad \text{Eqn. 2-9}$$

Where α is Biot's constant.

2.1.4 Thermoelastic Stress

During waterflooding, injection fluids that are cooler or hotter than the rock will result in changes in the temperature around the wellbore and therefore considerably alter the geomechanical stress distribution, which in turn would affect the change of parting pressure of the reservoir rock or variation of the geometry and direction of propagation of induced fractures. For example, injection of cooler fluids causes the rock grains and matrix to contract, in which leads to a decrease of thermo-elastic in the rock stress. The corresponding lowering of the tangential stress will promote formation fracturing (Sadd 2009). This is referred to as injection induced thermoelastic stress (Perkins and Gonzales et al., 1985; Garon et al., 1988; Clifford et al. 1991).

Perkins and Gonzalez (1985) showed that with injection induced fracture, thermoelastic stress at fracture tip was affected by the geometry of cooling region in storage aquifer with finite thickness

$$\Delta\sigma^T = S_f \frac{\alpha_T E \Delta T}{1-\nu} \quad \text{Eqn. 2-10}$$

Where,

ΔT: the temperature difference between injected fluid and formation temperature, °F

S_f: the geometric shape factor for the shape of the cooled region of reservoir rock

In Perkins and Gonzalez study, S_f can be obtained as:

$$S_f = \frac{(b_0/a_0)}{1+(b_0/a_0)} \quad \text{Eqn. 2-11}$$

Where a_0 and b_0 are major and minor semi-axis of an elliptical cooling region, respectively. Charlez (1997) published the α_T values in the range of 1.34 psi/°F to 29.16 psi/°F, and Hettema, Bostrøm, and Lund (2004) estimated the range for sandstone formations in the GoM, from 2.77 psi/°F to 8.33 psi/°F.

2.1.5 Water Quality

In waterflooding, water quality is usually defined in terms of the plugging tendency of the water. Ideally, the quality of the water should be such that there is no reservoir plugging, and hence no loss of injectivity during the life of the flood. However, poor injection water quality (as measured by its content of suspended solids or oil) causes the reduction in injectivity in many water injection wells.

2.2 Hydraulic Fracturing Mechanism

2.2.1 Initiation of Hydraulic Fracturing

There are three ways of applying a force to enable a fracture to propagate as shown in **Figure 2-3**:

1. Mode I – Opening mode (a tensile stress normal to the plane of the fracture)
2. Mode II – Sliding mode (a shear stress acting parallel to the plane of the fracture and perpendicular to the fracture front)
3. Mode III – Tearing mode (a shear stress acting parallel to the plane of the fracture and parallel to the fracture front)

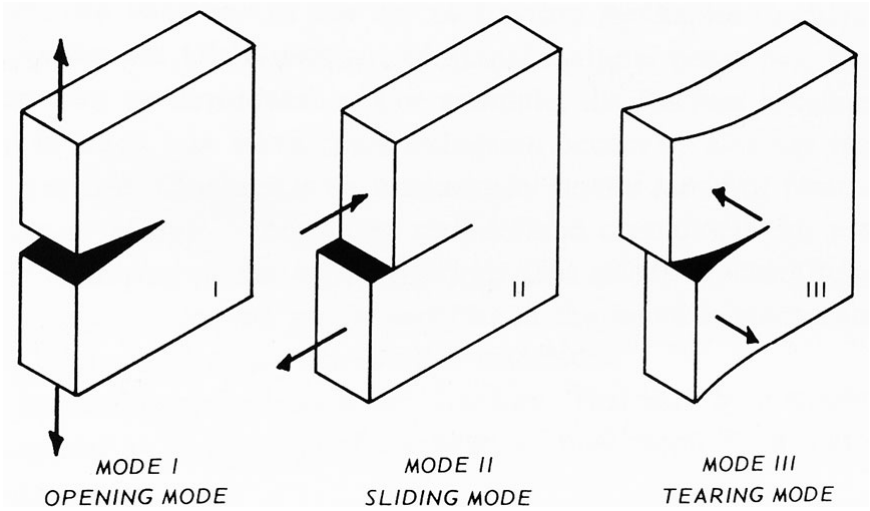

Figure 2-3 Different mode of the initiation of hydraulic fracturing. Excerpted from Edwalds and Wanhill (1984).

Since most of conventional fracture models assume Mode I fracturing, in this project, the initiation of Mode I fracture, tensile open fracture, in normal faulting stress regime ($\sigma_{H,min} < \sigma_{H,min} < \sigma_v$) is considered. The initiation of formation tensile fracture requires that the effective tangential stress must exceed the formation tensile strength. For isotropic

stresses, the upper limit of the imposed pressure required to fracture a formation from a vertical wellbore is given by the Terzaghi equation:

$$P_{bd} = 3\sigma_{H,min} - \sigma_{H,max} + \sigma_s - p \qquad \text{Eqn. 2-12}$$

The lower boundary for the breakdown pressure is:

$$P_{bd} = \frac{3\sigma_{H,min} - \sigma_{H,max} + \sigma_s - 2\eta p}{2(1-\eta)} \qquad \text{Eqn. 2-13}$$

Where,

$$\eta = \alpha \frac{(1-2\nu)}{2(1-\nu)} \qquad \text{Eqn. 2-14}$$

σ_s: the tensile strength of formation, psi

p: fluid pressure in the reservoir, psi

With the consideration of thermoelastic and poroelastic stress (Fjar, Holt, Horsrud, Raaen, & Risnes, 2008), the upper bound of the breakdown pressure is:

$$\mathrm{P_{bd}} = \frac{3\sigma_{H,min} - \sigma_{H,max} + \Delta\sigma^T + \Delta\sigma^P + \sigma_s}{2} \qquad \text{Eqn. 2-15}$$

The superscript T and P indicates that this pressure accounts for contribution of thermoelastic and poroelastic stress respectively. Usually, the breakdown pressure is greater than the fracture extension pressure. The breakdown pressure represents the pressure required to initiate a fracture from the wellbore and is influenced by the very presence of the wellbore. The fracture extension pressure reflects the pressure required to propagate the fracture through the formation.

2.2.2 Fracture Gradient Determination

Methods for estimating fracture pressure gradient can be classified as direct methods and indirect methods. Direct methods rely on measuring the pressure required to fracture the rock and the pressure required to propagate the resulting fracture. They are generally based on a field procedure called leak-off test and use mud to pressurize the well until formation fracture is initiated. A leak-off test (LOT) is a normal procedure in vertical wildcat wells where the formation fracture gradient is not well established. During the test, the well is shut in and fluid is pumped into the wellbore at constant injection rate to gradually increase the pressure. At some pressure, fluid will enter the formation, or leak off, either moving through permeable paths in the rock or by creating a space by fracturing the rock. A typical leak-off test procedure is illustrated in **Figure 2-4**, where the breakdown pressure is a direct measurement of the fracturing pressure, and the closure stress is the minimal earth stress. The difference between the breakdown and closure stresses is the stress needed to overcome any additional hoop stress at the wall plus the tensile strength of the formation rock. This difference may be small in many cases, including those involving overpressure, fractured, or ductile formations. As with the pore pressure, such direct measurements of the fracture gradient are not routinely available; thus, estimates for the minimum principal in-situ stress and breakdown pressure based on other measurements are sought.

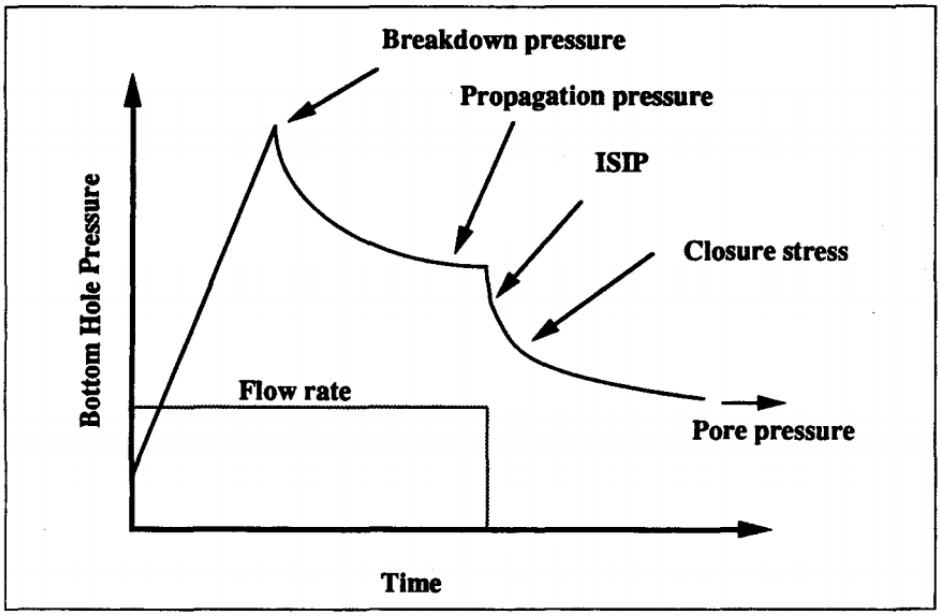

Figure 2-4 The process of the hydraulic fracturing and the determination of the formation parting pressure from field test.

Several studies have been carried out to predict formation fracture gradients and some often-used methods are discussed as follows.

2. 2. 2. 1 Hubbert and Willis Method

Hubbert and Willis (1957) developed an equation to predict the pressure required to fracture a formation. Their theory is based on laboratory tri-axial compression tests and can be applied to tectonically relaxed areas with normal faulting. Their model was the basis for future methods, and it basically states that the fracture pressure is equal to the minimum horizontal stress plus the formation pore pressure. The minimum horizontal stress is equal to some fraction of the effective vertical stress, which is the overburden pressure minus the formation pore pressure. This minimum horizontal stress is about 1/2 to 1/3 of the effective vertical matrix stress. The resulting equation is

$$\frac{\mathrm{F}}{D} = \left(\frac{1}{3}\ to \frac{1}{2}\right)\left(\frac{S}{D} - \frac{P}{D}\right) + \frac{P}{D} \qquad \text{Eqn. 2-16}$$

This equation is also based on the assumption that the overburden pressure gradient approximates 1.0 psi/ft. Although this model is the cornerstone for other methods, it is not widely utilized, due to the low values it normally yields because of the assumption of a constant stress ratio of 1/3 to 1/2 of the vertical stress.

2. 2. 2. 2 Matthews and Kelly Method

Matthews and Kelley (1967) presented a fracture gradient equation similar to Hubbert and Willis equation. In it, they developed the concept of variable ratio between the effective horizontal and vertical stresses:

$$\frac{\mathrm{F}}{\mathrm{D}} = K_i\left(\frac{S}{D} - \frac{P}{D}\right) + \frac{P}{D} \qquad \text{Eqn. 2-17}$$

where the coefficient, K_i, relates the actual matrix stress conditions of the formation of interest to the conditions of matrix stress if the formation is compacted normally. Values for K_i are determined empirically from known fracture initiation pressures for an area.

The Matthews and Kelly approach showed two weaknesses. One is the assumption that overburden stress is 1.0 psi/ft of depth. The other is that the stress ratio used in calculating the fracture gradient in abnormally pressured formations is that of the deepest normally pressured formation.

2. 2. 2. 3 Ben Eaton Method

Eaton (1969) expanded on the work of Hubbert and Willis by formally introducing Poisson's ratio, and a variable overburden gradient. The amount of horizontal stress caused by the vertical matrix stress is a function of Poisson's ratio v of the rock in question and is expressed in the form of

$$\sigma_{\mathrm{H}} = \frac{\nu}{1-\nu}\sigma_v \qquad \text{Eqn. 2-18}$$

The resulting fracture pressure gradient equation is:

$$\frac{\mathrm{F}}{\mathrm{D}} = \frac{\nu}{1-\nu}\left(\frac{S}{D} - \frac{P}{D}\right) + \frac{P}{D} \qquad \text{Eqn. 2-19}$$

2.2.3 Fracture Propagation Process

Once the fracture initiation pressure is exceeded, the rock fractures instantaneously and continuously. The length of the fracture will depend on both rock properties (particularly the tensile strength), the fluid pressure applied in the wellbore, and the magnitude of the minimum horizontal stresses. It is expected that when the tensile strength is low, the horizontal stresses are low, and the well is pressurized at a high pump rate, then the extent (length) of the initial fracture will be high. The reverse is expected for a rock with high tensile strength. After the fracture initiation, the pressure builds up in the fracture until it exceeds the fracture propagation pressure and then the fracture propagates. This propagation is accompanied by pressure drop which is due to the formation of a large fracture surface over a relatively short period of time, and also due to other processes such as fluid leak-off and frictional losses. Thus, the fracture propagation process can be

considered to be a series of pressure build-up, fracture propagation, and pressure decline cycles.

2.3 Fracture Geometry Models

There are various hydraulic fracturing models used to approximately define the development of fracture geometry. Improvement of the computer modeling is an important component that is able to accurately predict the fracture growth and dimensions for a given injection rate, time and fluid leak off. Initially hydraulic fracturing used two dimensional models (2D) which normally have fixed fracture height. From these models, more complex pseudo three-dimensional (P3D) and three-dimensional (3D) models have evolved which have the advantage of more computing power. In this research, a 2D model is adopted to determine the fracture geometry. P3D models are generally a more realistic representation of hydraulic fracture than the 2D models for most situations because the P3D model includes the fracture height, width, and length distribution with the data for the pay zone and all the rock layers above and below the perforated interval. Because of its complexity and availability in most commercial software, the P3D model is not discussed here. Some notable 2D models are described in following sub sections.

2.3.1 KGD and PKN Models

There have been numerous theories proposed for hydraulic fracturing in rocks (Harrison et.al, 1954, Hubbert and Willis, 1957 and Economides, 1995). Traditionally, Griffith-Sneddon formed the basis of most fracture geometry models (Economides, 1995). Their work then was expanded by Perkins and Kern (1961). Later on Nordgren (1972) modified the PK model to include the effects of fluid loss into formation. The PKN model as shown

in **Figure 2-5** is applied to the fractures in vertical plane. It has an elliptical shape and the maximum width at the center as shown in **Figure 2-6**. It assumes that fracture has a fixed height independent of fracture length and the length is much greater than height. It also assumes that the fluid flow and fracture propagation are one-dimensional in a direction perpendicular to the elliptic cross-section.

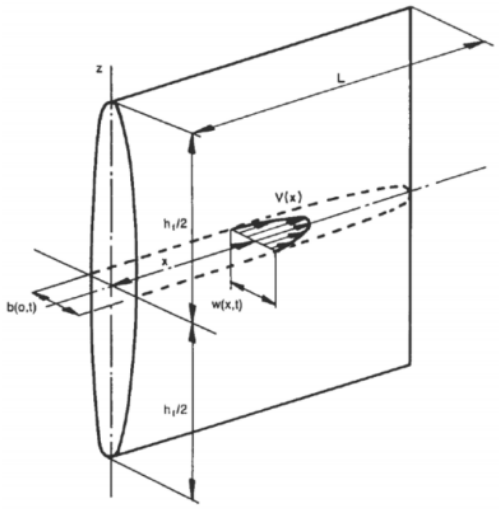

Figure 2-5 the geometry of PKN model (Gidley, Holditch, Nierode, & Jr., 1989)

Khristianovic and Zheltov (1955) and Geertsma and De Klerk (1969) developed another fracturing model, assuming horizontal plane strain condition often referred to as the KGD geometry (**Figure 2-6**). The KGD model is applicable for short fractures where the assumptions of plane strain are applied to horizontal sections. This model is applied to the fractures in vertical planes. It assumes that fracture has a fixed height and height is greater than the fracture length. It has a rectangular cross-section of the fracture. It also assumes that fluid flow and fracture propagation are one-dimensional in a direction perpendicular to the rectangular cross-section. Rock stiffness is taken into account in 2D

plane strain deformation in the horizontal plane only, so each horizontal cross-section deforms independently from the other (Gidley et al., 1989)

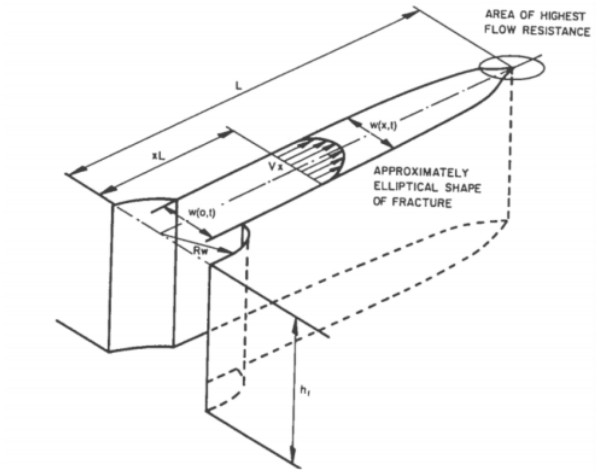

Figure 2-6 the geometry of KGD model (Gidley et al., 1989)

2.3.2 Perkins and Gonzalez Model

The Perkins and Gonzalez model considers thermal stress and pore pressure change during injection. Thermoelastic stresses for a region with an elliptical cross-section and finite thickness are determined approximately with a numerical procedure. Empirical equations were developed to estimate the average interior thermal stresses in elliptical cooled regions of any height. Stress changes induced by pore pressure changes during fracturing are calculated using a similar equation with thermal stresses by assuming linear elasticity. The computed thermal stresses and stress changes due to pore pressure changes are coupled with solutions for a PKN hydraulic fracturing model to determine fracture dimensions – including length and width as functions of injection volume or time. Examples using typical elastic and thermal properties showed that injection of cool water can reduce in-situ stresses around injection wells substantially, causing them to fracture

at pressures considerably lower than would be expected in the absence of the thermoelastic effect.

When water is injected during waterflooding, a region of cooled rock forms around the injection well. This region grows as additional water is injected. At any time, its outer boundary is approximately elliptical that is confocal with the line crack (2D fracture) as shown in **Figure 2-7**.

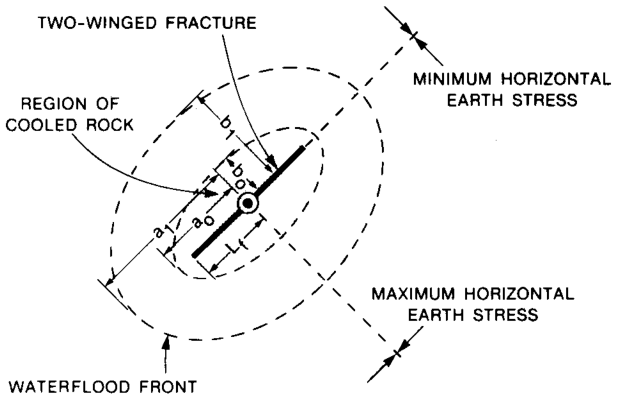

Figure 2-7 Three regions of Perkins and Gonzalez Model as the result of water injection (Perkins & Gonzalez, 1985)

Three zones with sharply defined boundaries are assumed:

1. The cooled-and-flooded ellipse from the wellbore out.

2. Followed by a flooded, but not cooled ellipse (the same temperature as the virgin reservoir, but increased injection water saturation).

3. The undisturbed virgin reservoir.

Thermoelastic stresses for regions of elliptical cross-section and finite thickness were determined approximately with a numerical procedure. The empirical equations to estimate the average interior thermal stresses in elliptical cooled regions are available in

literature. One must note that the pressure in the elliptical region is not uniform and stress changes due to pore pressure changes may have to be computed from a reservoir model. For a fractured injection well, the injected (flooded) region is approximately elliptical in shape, in its plan view, and it is confocal with the fracture length. The size of the elliptic region, its major and minor semi-axes, can be determined from volume balance of the injected water. The cooled region is also approximated as elliptical in cross-section, and is also confocal with the fracture; the major and minor semi-axes of the cooled region are determined from an energy balance. Heat transfer and energy loss to the upper/lower bounding layers are not considered in their original model.

When the fracture length is short, the shape of flooded and cooled region is close to a circular shape, and the thermally-related reduction of the horizontal stresses is nearly uniform in all directions. As the fracture length becomes large, the cooled region becomes more elongated. As the cooled region lengthened, the thermal stress reduction parallel to the fracture exceeds the thermal stress reduction perpendicular to the fracture. This tends to reduce the difference between stresses within the cooled region and it is possible at some point the stress parallel to the fracture becomes as large as the stress perpendicular to the fracture. When this happens, fractures may initiate along the original fracture surface and propagate in the direction perpendicular to the original fracture. Whether this will happen or not depends on the difference in the principal horizontal stresses that are initially present in the reservoir, the thermal coefficient of expansion, the temperature change and the elastic modulus. This process is depicted in **Figure 2-8**.

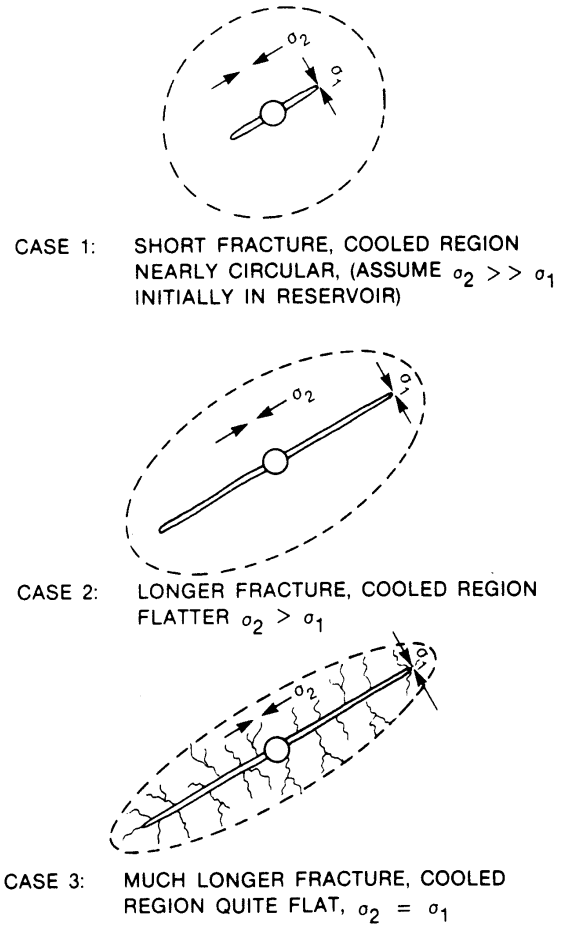

Figure 2-8 The developed of regions for water injection process (Perkins & Gonzalez, 1985)

2.3.3 Koning's Model

Koning (1988) presented an analytical model of fracture growth in an infinite reservoir and in the absence of reservoir stress change in which the leak-off distribution in the reservoir is allowed to range from 1-D perpendicular to 2-D radial with respect to fracture. In his dissertation, Koning also presented an analytical model for fracture propagation in an infinite reservoir under the influence of poroelastic and thermoelastic changes in rock to characterize features of injection-induced fracture growth. The assumption within the model are listed as follows:

1) A vertical fracture with a rectangular surface area having height h and half- length L extends laterally from a single well in an infinite reservoir. The reservoir and fracture heights are constant. The shape of the fracture is elliptical.
2) By assuming infinite conductivity fracture, the fluid pressure drop along the fracture can be neglected.
3) Similar to Perkins and Gonzalez model, the shapes of the fronts that separate the cold-flooded and the warm-flooded parts of the reservoir are approximated by ellipses that are confocal with the fracture tips at all times.

After that, Ovens and Niko (1993) formulated a radial version of Koning's model. They combined the fracture growth criterion with thermal and poroelastic effects and fracture toughness to yield a compact formulation, relating changes in fracture length to changes in fracture pressure.

2.4 Injectivity Before and After Formation Fractured

Well injectivity measures the ability of an injection well to receive injected fluid. The injectivity index, J, of an injection well is simply defined as:

$$\mathrm{J} = \frac{\mathrm{Q}}{P_e - P_{wf}} = \frac{kh}{141.2\mu B(\ln\frac{r_e}{r_w} + s)} \qquad \text{Eqn. 2-20}$$

Where,

Q: surface flowrate at standard conditions, STB/D

P_e: external boundary radius pressure, psi

P_{wf}: bottom hole flowing pressure, psi

r_w: wellbore radius, ft.

r_e: drainage radius, ft.

μ: viscosity, cp

s: total near-wellbore skin factor

While the fracture grows into the reservoir, the well injectivity is improved, restoring the initial injectivity index. This phenomenon must be included in the injectivity index calculation thorough the geometrical factor, calculating the formation damage factor due to fracture, s_f. There are models to calculate the formation damage factor for hydraulic fracturing after a stimulation procedure, but there are not exclusive models to use with fractures induced by water injection. In fracture regime, injectivity of a well can be defined in a similar fashion. Agarwal, Gardner, Kleinsteiber, and Fussell (1998) and Cinco-Ley (1981) introduced the fracture dimensionless conductivity, $C_{fD,}$ which is defined as:

$$C_{fD} = \frac{k_f w}{k x_f} \qquad \text{Eqn. 2-21}$$

In a cylindrical coordinates the pseudosteady-state flow equation for a hydraulically fractured oil well is:

$$q = \frac{kh(\bar{p} - p_{wf})}{141.2B\mu\left[\ln\left(\frac{r_e}{r_w}\right) - 0.75 + s_f\right]} \qquad \text{Eqn. 2-22}$$

Using the concept of equivalent radius as follows,

$$r_w' = r_w e^{-s_f} \qquad \text{Eqn. 2-23}$$

we have

$$r'_w = \frac{x_f}{\frac{\pi}{C_{fD}} + 2} \qquad \text{Eqn. 2-24}$$

From the equation above, the equivalent skin effect, s_f can be obtained and thus the flow equation as well as injectivity index could also be evaluated.

Chapter 3: Relationship Between Injection Pressure and Rate for an Injection Well

For an injection process, usually the known parameters include surface pump pressure and injection rate, and from which we would be able to determine whether the injection is above or below formation parting pressure, or to determine if the water is injected through a fracture or into formation matrix. From the pump pressure to formation sand face, there are several hydraulic pressure changes should be considered as presented below.

Bottomhole pressure data at the formation face is required in the process and interpretation of injection data. Bottomhole pressure depends on the surface pressure, pressure drop due to friction along the tubing, the hydrostatic head and any pressure drop through the completion system that is in place. Considering the injection string to start with, the pressure change through the tubing or the annulus is governed by potential energy, kinetic energy, and frictional contributions. With a few exceptions (e.g. high rate flow through elbows, restrictions), kinetic energy terms are usually ignored. Considering a simple situation: a single-phase flow, ignoring acceleration effects, the bottomhole pressure can be estimated from surface pressure as follows:

$$BHP = P_{surface} + P_{hydrostatic} - P_{friction} \quad \text{Eqn. 3-1}$$

Where:

BHP: bottomhole pressure at the formation face, psi

$P_{surface}$: surface pressure, psi

$P_{hydrostatic}$: hydrostatic head due to the fluid column, psi

$P_{friction}$: frictional pressure drop through tubing, completion and perforations, psi

3.1 Friction in the Injection String

The pressure drop due to friction along tubing per unit length is:

$$\frac{\mathrm{dP}}{\mathrm{dL}} = 0.3813 \frac{f \rho q^2}{D^5} \qquad \text{Eqn. 3-2}$$

During flow, irreversible energy losses occur. Except for completely laminar flow, these energy losses cannot be predicted theoretically and are usually accounted for by using the friction factor. For consistency, the Moody friction factor is used in this study. The friction factor, f, and the relative roughness (ε/D) are related to the Reynolds' Number. The Reynolds' Number is defined as follows:

$$\mathrm{N_{Re}} = 7737.6 \frac{D \times v \times S.G.}{\mu} \qquad \text{Eqn. 3-3}$$

Where,

dP: pressure change, psi

dL: length of the segment over which the pressure drop is calculated, ft.

ρ: density, $\mathrm{lbm/ft^3}$

f: Moody friction factor, dimensionless

q: injection rate, BPM

v: velocity, ft/s

D: diameter: inches

The friction factor depends on the specific flow regime Except for laminar flow, there are many empirical representations of the friction factor in turbulent and transitional regimes. The following formulae are used in the study.

Table 1. Moody Friction Factors

Flow Regime	Reynolds Number	Moody Friction Factor	Comments
Laminar flow	< 2100	$f_{\mathrm{M}} = \frac{64}{N_{\mathrm{Re}}}$	Independent of roughness
Turbulent flow	> 2100	$\frac{1}{\sqrt{f_M}} = 1.74 - 2\log\left(\frac{2\varepsilon}{D} + \frac{18.7}{N_{\mathrm{Re}}\sqrt{f_M}}\right)$	Colebrook-White

3.2 Static Bottomhole Pressure and Hydrostatic Head

To convert surface pressure to bottomhole pressure, the friction is calculated first. Then the hydrostatic head is determined. For a liquid, the static bottomhole pressure or hydrostatic head is determined by multiplying the fluid gradient times the depth:

$$\mathrm{P_{hydrostatic}} = \mathrm{TVD} \times \mathrm{gradient} \qquad \text{Eqn. 3-4}$$

The gradient can be determined from the specific gravity of the fluid:

$$\mathrm{gradient\ (psi/ft)} = \frac{\mathrm{S.G.} \times 62.4}{144} = \mathrm{S.G.} \times 0.433 \qquad \text{Eqn. 3-5}$$

3.3 Injected Fluid Hydraulic Properties

The injection water viscosity is calculated from the following correlation as a function of temperature, pressure and solids in injection water. The relationship between viscosity and temperature with the influence of solids in injection water is illustrated in **Figure 3-1**.

$$\mu = -4.518\times10^{-2} + 9.312\times10^{-3}TDS - 3.93\times10^{-4}TDS^2 + \left\{\frac{70.635 + 9.3576\times10^{-2}TDS^2}{T_i}\right\}\{1 + 3.5\times10^{-12}(P_i + 14.696)^2(T_i - 40)\} \quad \text{Eqn. 3-6}$$

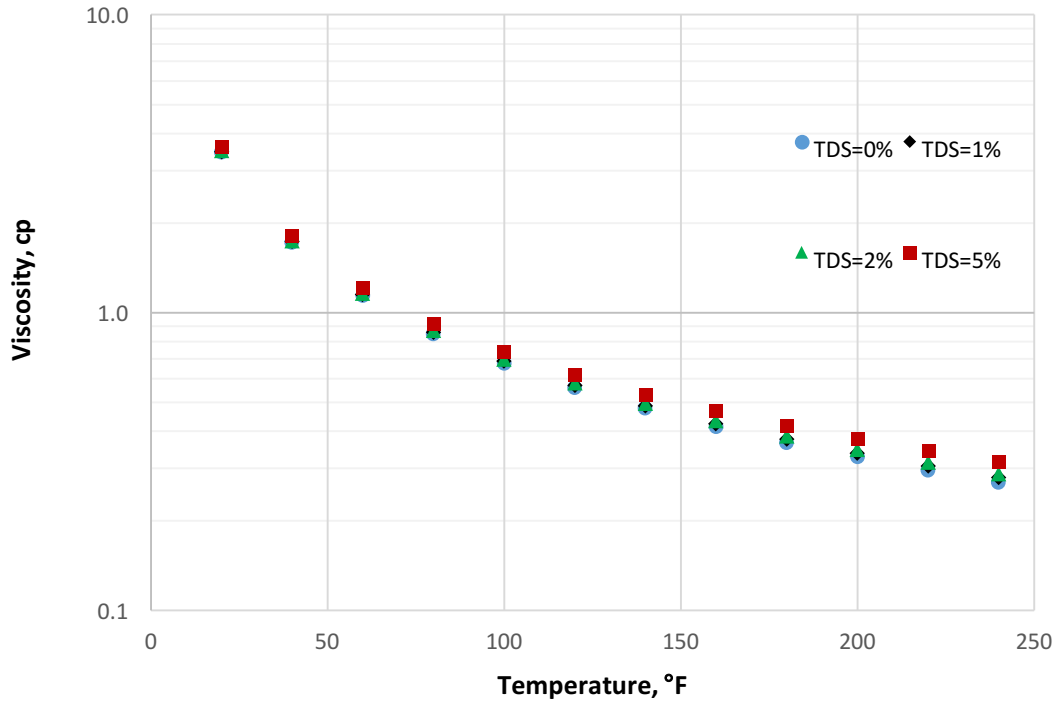

Figure 3-1 Water viscosity vs. temperature with the existence of solids

The specific gravity of the injected fluid is calculated from following correlations:

$$S.G. = (7.572\times10^{-3}TDS + 0.998238)\times1.002866e^{\psi} \quad \text{Eqn. 3-7}$$

$$\psi = 3.0997\times10^{-6}\left(\frac{P_i + P_{wellhead}}{2}\right) - 2.2139\times10^{-4}(T_i - 59) - 5.0123\times10^{-7}(T_i - 59)^2 \quad \text{Eqn. 3-8}$$

Where,

TDS: total dissolved solids in the injection water, percentage

T_i: injection water temperature, °F

P_i: bottomhole injection pressure, psi

$P_{wellhead}$: wellhead injection pressure, psi

Figure 3-2 demonstrates the relationship between specific gravity of water and temperature under different solids concentration conditions.

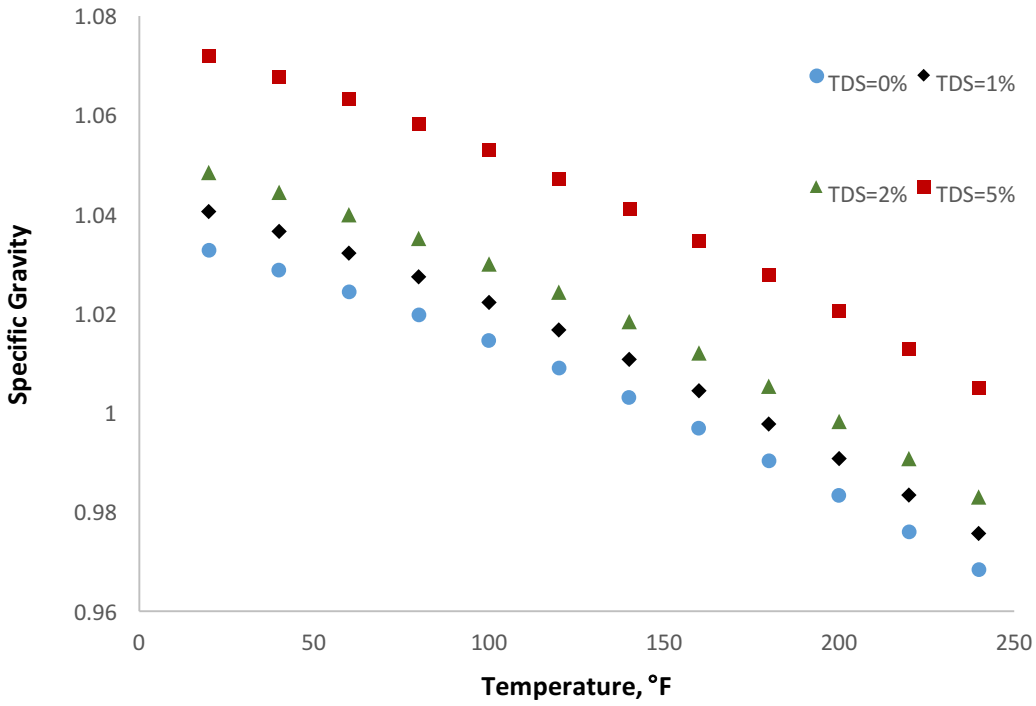

Figure 3-2 Specific gravity of water with various solids concentrations

The hydrostatic head is determined from the specific gravity, at the datum, z_{datum} (ft.):

$$P_{hydrostatic} = 0.433 \times z_{datum} \times S.G. \qquad \text{Eqn. 3-9}$$

3.4 Perforation Friction

Analysis of field and laboratory data shows that variations in pressure drop due to changing perforation entry friction tends to strongly influence the prediction of fracturing treatment performance (Crump & Conway, 1988).

The formula adopted by Crump and Conway is:

$$P_f = \frac{0.2369 Q^2 \rho}{N_p^2 D^4 C_d^2} \qquad \text{Eqn. 3-10}$$

Where,

Q: flow rate, BPM

ρ: fluid density, lbm/gal

N_p: number of perforations

D: perforation diameter, inches

C_d: coefficient of discharge

3.5 Model Description

A fracture and water injection model is programmed for the study with following features:

1) Various pressure losses such as frictional loss along the tubing and friction due to perforation are considered explicitly.
2) Both matrix injection with formation damage and fracturing injection are considered.
3) The fracture is assumed to have a constant fracture height.
4) Stress changes due to temperature and pore pressure changes are considered.
5) Formation damage due to injection water quality such as total suspended solids oil in water is considered.
6) The well can be vertical or deviated.
7) Monte Carlo analysis is used to determine the distribution of fracturing pressure.

The program requires a large number of input parameters including reservoir petrophysical and geomechanical properties, injected fluid quality, well data as well as tubing settings. The calculated data include injection pressure (bottomhole pressure and

wellhead injection pressure), well injectivity, whether it is under matrix injection or fracturing injection. If the injection is under fracturing condition, the fracture properties such as fracture length, fracture net pressure, and fracture skin are calculated. The parameters and calculation procedures are discussed in detail in following sub sections.

3.5.1 Propagation Calculations

In the developed model, the pressure change due to pore pressure change is modeled as follows through the poroelastic coefficient, A_p, which is defined as:

$$A_p = \beta\alpha\frac{1-2\nu}{1-\nu} \qquad \text{Eqn. 3-11}$$

Where,

β: Perkins and Gonzalez shape factor,

α: Biot's poroelastic parameter,

ν: Poisson's ratio.

The injection shape factor, β, is derived from the work of Perkins and Gonzalez to characterize the portion of the reservoir influenced by fluid injection and temperature changes. The shape factor ranges from 0 (when a small region on each side of a fracture has been cooled) to 0.5 (when a small radial distance from the wellbore has been cooled) to 1.0 when the degree of cooling is large enough that the extent of the thermal front is greater than the formation height or greater than the half-length of a created fracture.

Similarly, the thermoelastic coefficient, A_t, is defined as:

$$A_t = \frac{\beta E \alpha_t}{1 - \nu} \qquad \text{Eqn. 3-12}$$

where:

E: Young's Modulus,

α_t: Coefficient of linear thermal expansion.

The current stresses in the near-wellbore/fracture region are determined for various scenarios as follow:

1) For no injection condition, the total stress is represented as:

$$\sigma = \sigma_0 + A_p(p_e - p_0) \qquad \text{Eqn. 3-13}$$

Where,

σ: current stress, psi

σ_0: original stress, psi

A_p: poroelastic coefficient

p_e: the current average reservoir pressure, psi

p_0: the original reservoir pressure, psi

This is essentially the original stress field plus changes in stress associated with the change in pore pressure.

2) If injection is occurring but the zone is not fractured, the stress acting is (initial stress, modified for changes in the stress due to changes in the reservoir pressure before injection, further modified by changes in the stress due to changes in pore pressure and temperature due to injection):

$$\sigma_{radial} = \sigma_e + A_p(p_e - p_0) + A_p(p_i - \Delta p_{skin} - p_e) \quad \text{Eqn.3-14}$$

Where,

p_i: injection pressure, psi

σ_e: current far-field stress, psi

Δp_{skin}: mechanical skin (accounts for any entry pressure drop), psi

3) If injection related fracturing is occurring and there are ongoing tests for this to see if the current stress level is exceeded by the injection pressure, the current stress field becomes:

$$\sigma_{\text{frac}} = \sigma_0 + \xi A_p(p_i - p_e) + A_t(T_{\text{i}} - T_0) \quad \text{Eqn. 3-15}$$

Where the correction factor ξ (from Koning (1988)) is defined as:

$$\xi = \left(1 - \frac{0.25}{\ln(2\,r_e/x_f)}\right)\left\{1 + 2\sinh^{-1}\left[\frac{2h_f}{x_f}\right] - 2\sinh^{-1}\left[\frac{h_f}{r_e}\right]\right\} \quad \text{Eqn. 3-16}$$

Where,

Δp_{skin}: specified mechanical skin (set to zero if the well is fractured), psi

ξ: correction factor (from Koning (1988)) to account for the finite nature of the reservoir

h_f: fracture height, ft.

x_f: fracture half-length, ft.

Furthermore, a condition check whether the formation is under matrix or fracturing injection is performed. The relation in **Eqn. 3-19** is to examine whether the formation face pressure exceeds the value required for fracturing:

$$p_i - \Delta p_{skin} > \sigma_{frac} \qquad \text{Eqn. 3-17}$$

If the relation is true, fracturing would occur and the formation face pressure shown on the left-hand side of the preceding equation is set to the fracturing pressure. Otherwise, radial flow is taken to be true. The fracture opening pressure is calculated as:

$$\mathrm{P_{opening}} = \sigma_0 - A_p P_0 + A_t(T_i - T_0) + \frac{A_p P_e(1-\xi)}{1 - A_p \xi} \qquad \text{Eqn. 3-18}$$

3.5.2 Injection Performance Calculations

The injection performance calculations are as follows:

$$\Delta p = p_i - p_e \qquad \text{Eqn. 3-19}$$

Use high mechanical skin to estimate the effect of water quality on the injectivity of unfractured zones. There is a conditional statement for calculating the Injectivity Index for pseudo-steady-state conditions in radial flow.

If $h_f = 0$, the Injectivity Index is calculated as:

$$II_{Matrix} = \left[\frac{kk_r h_{net}}{141.2\mu \ln(r_e/r_w) + s_m + s_g - 0.75}\right]/x \qquad \text{Eqn. 3-20}$$

Where

$$x = 1 + 22e^{-kk_r/22} \times (0.05TSS + 0.0007OIW) \qquad \text{Eqn. 3-21}$$

$$q_{Matrix} = \Delta p II_{Matrix} \qquad \text{Eqn. 3-22}$$

Alternatively, if it is determined that the well is fractured, etc., $h_f > 0$, the fractured

Injectivity Index is calculated as:

$$II_{fracture} = \left[\frac{kk_r h_{net}}{141.2\mu \ln(r_e/r_w) + s_g - 0.75}\right]/x \qquad \text{Eqn. 3-23}$$

Where,

$$x = 1 + 22e^{-kk_r/22} \times (0.05TSS + 0.0007OIW) \qquad \text{Eqn. 3-24}$$

$$q_{fracture} = \Delta p II_{fracture} \qquad \text{Eqn. 3-25}$$

Finally, a "total" injectivity index is determined by adding matrix and fractured components and similarly a total rate is determined, all iteratively.

If the well is deviated, the skin due to the well deviation is calculated as

$$s_g = \left(\frac{\theta'}{41}\right)^{2.06} - \left\{\left(\frac{\theta'}{56}\right)^{1.865} \log\left(\frac{h_g N_g}{100 r_w \sqrt{\frac{k_v}{k_h}}}\right)\right\} \qquad \text{Eqn. 3-26}$$

$$\theta' = \tan^{-1}\left(\left(\frac{k_v}{k_h}\right)^{1/2} tan\theta\right) \qquad \text{Eqn. 3-27}$$

Where,

θ: deviation of the wellbore from the vertical through the zone, degree

h_g: the gross thickness of the zone, ft.

N_g: the ratio of the net to the gross thicknesses

k_v: vertical permeability, mD

k_h: horizontal permeability, mD

3.5.3 Fracture Properties Calculations

The skin factor due to hydraulic fracture is given as:

$$S_f = \ln\left(\frac{2r_w}{x_f}\right) \quad \text{Eqn. 3-28}$$

If a fracture exists, its total fracture height is assigned to the gross height of the zone ($h_f = h_g$). Knowing the bottomhole pressure, the net pressure is then calculated. The net pressure is determined as the treating pressure downstream of any completions minus the current in-situ stress level which accounts for evolving poroelastic and thermoelastic effects:

$$p_{net} = p_i - \sigma - \Delta p_{skin} \quad \text{Eqn. 3-29}$$

In the fracture, we assume that the pressure changes linearly from tip to tip because of its high conductivity. The fracture friction is calculated as:

$$p_{friction} = \frac{p_{net}}{x_f} \quad \text{Eqn. 3-30}$$

The fracture length in this program is determined by iterating until the pressure drop along the fracture length is between 3.5 and 4 psi/ft and the wellhead target pressure is matched. The injection gradient is calculated as the bottomhole pressure divided by the depth. The fracture gradient is calculated as the fracture opening pressure divided by the depth.

3.5.4 Tubing Friction Calculations

The friction along the tubing is determined in one of the calculation routines in the programing. Up to ten different strings can be included. For each string, tubing ID, tubing length and absolute roughness are specified.

As mentioned in Chapter 3.1, the friction factors for laminar and turbulent flow are conditionally calculated as follows:

1) For a nonzero flow, $f = 64/N_{Re}$ for laminar flow.
2) For a nonzero flow, and a Reynolds number in greater than 2100, the turbulent friction factor is iteratively calculated from the Colebrook White equation, by minimizing the following error:

$$error = 1 + 2\sqrt{f}\log\left(\frac{\varepsilon}{3.7\left(d_{tubing}/12\right)}\right) + \left(\frac{2.51}{N_{re}\sqrt{f}}\right) \qquad \text{Eqn. 3-31}$$

Friction is then calculated conditionally as:

1) For laminar flow ($N_{Re} < 2100$),

$$\Delta p_{friction} = \frac{0.001295 \times f_{laminar} \times z_{tubing} \times v^2 \times S.G. \times 62.4}{d_{tubing}} \qquad \text{Eqn. 3-32}$$

2) For turbulent flow ($N_{Re} > 2100$),

$$\Delta p_{friction} = \frac{0.001295 \times f_{turbulent} \times z_{tubing} \times v^2 \times S.G. \times 62.4}{d_{tubing}} \qquad \text{Eqn. 3-33}$$

Where,

f: friction number

z_{tubing}: tubing length, ft.

d_{tubing}: tubing ID, inch

v: velocity, ft/s

S.G.: fluid specific gravity

ε: absolute roughness, ft.

Finally, friction for each tubing section is summed up as total friction.

3.6 Iteration Procedures

Based on the model discussed above, the following iteration procedure is proposed to determine the relationship between the pump pressure and injection rate before and after formation fracturing. The whole iteration procedure is divided into 3 steps and will be discussed in detail below. A detailed iteration flowchart is shown in **Figure 3-6**.

Step 1: To initiate homogeneous calculations, a small fracture is considered in the layer. The fracture half-length is set to be twice the wellbore radius. Consequently, fracture skin is defaulted to zero in the radial flow equations assuming an infinite conductivity fracture.

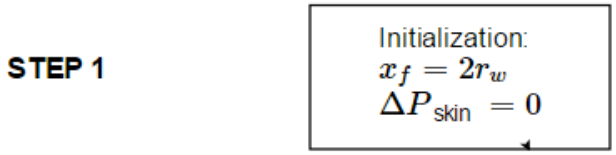

Figure 3-3 Calculation procedure Step 1: initialization

Step 2: Injection rates and bottomhole pressures derived at this stage are for injection under matrix conditions without fracturing. The following calculations are made:

1. Given a bottomhole pressure (from initial reservoir pressure, P_i), a rate (in radial flow) is calculated.
2. From this rate, a pressure drop due to friction along the tubing is calculated.
3. The wellhead pressure is then derived from the bottomhole pressure minus the hydrostatic head and plus the frictional pressure drop.
4. The calculated wellhead pressure is then compared to the target wellhead pressure entered by the user and the operation is then iterated until these values match.
5. The user has entered a target wellhead injection pressure and the calculated wellhead injection pressure is iteratively compared with this until convergence is achieved – an error is also reported indicating the difference between the calculated and targeted values. The wellhead injection pressure is calculated as the bottomhole pressure plus the friction pressure minus the hydrostatic head plus calculated friction
6. Once the wellhead pressure has been matched, the calculated bottomhole pressure is compared to the reservoir pressure and the stress. Three conditions are evaluated before moving to the last calculation step:
7. If the value of the bottomhole pressure does not exceed the reservoir pressure, then it is classified as no injection occurring.
8. If the value of the bottomhole pressure exceeds the reservoir pressure but does not exceed the current in-situ stress, a matrix injection condition is presumed to occur.
9. If the value of the bottomhole pressure exceeds both the reservoir pressure and the current in-situ stress, fractured injection condition is presumed to occur.

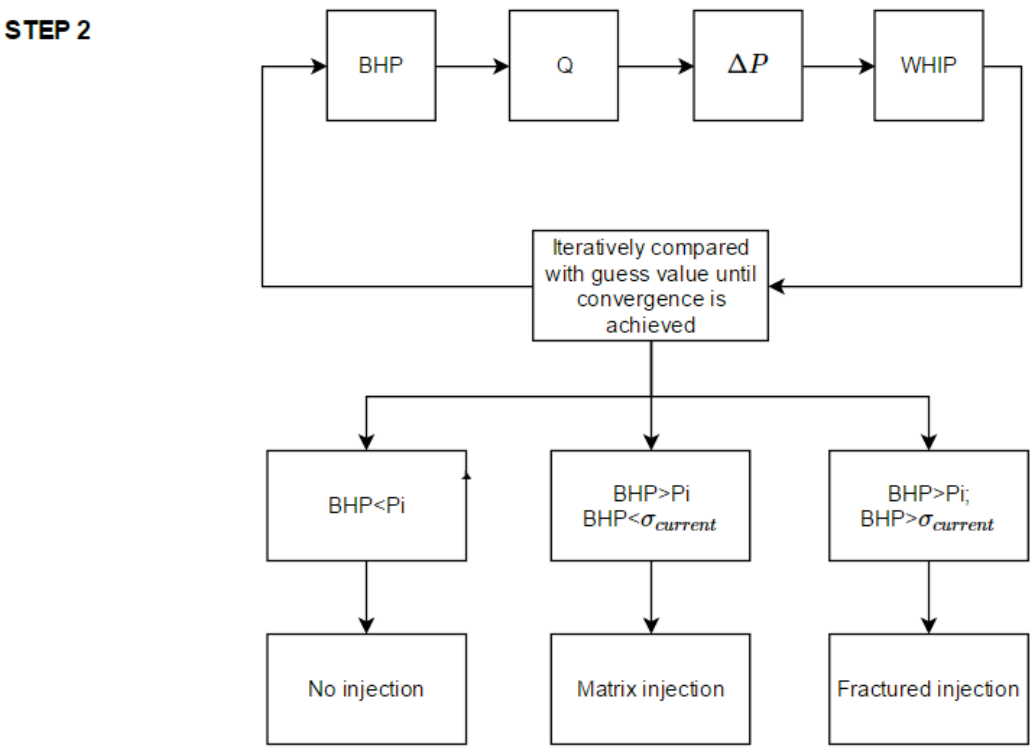

Figure 3-4 Calculation procedure Step 2: evaluate injection conditions

Step 3: This last step performs fracture calculations, to derive length, rate and pressure that have been indicated to be fractured (per the foregoing conditional statements).

1. First, the bottomhole pressure is again tested to ensure that it does exceed the relevant stress.
2. If this condition is unsatisfied, the calculation does not proceed and the results are unaltered from those previously determined in the second step.
3. If a fracturing condition is satisfied, the injection rate is calculated from the bottomhole pressure. Again, iterations are made to match the wellhead pressure based on the rate change.

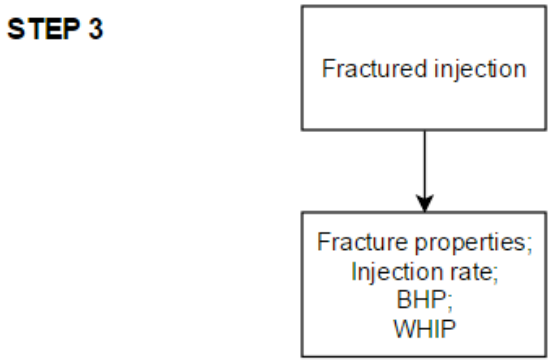

Figure 3-5 Calculation procedure Step 3: fracture calculations under fracturing condition

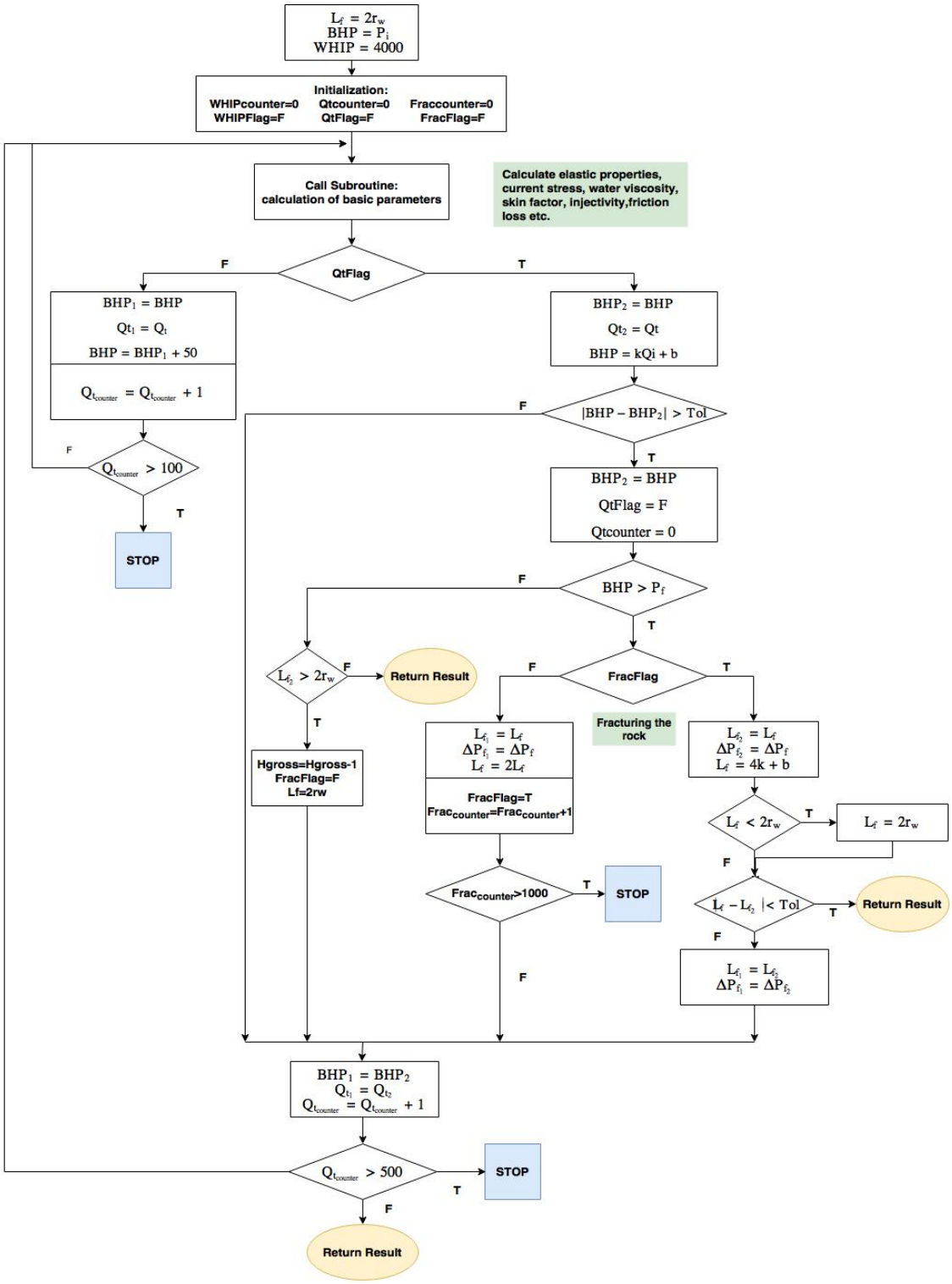

Figure 3-6 Iteration flowchart of calculation procedure

Chapter 4: Case Study on a GOM Deepwater Injection Well

4.1 Introduction of the field

Many deep-water discoveries in Gulf of Mexico in the past five years are in water depths greater than 4,000 feet and in older Tertiary reservoirs of middle Miocene to Paleocene (Liu, Dessenberger, McMillen, Lach, & Kelkar, 2008). The middle Miocene constitutes one of the most prolific hydrocarbon-producing intervals in the Gulf of Mexico. The middle Miocene depositional episode is bounded by regional-marine transgressive deposits and flooding surfaces associated with faunal tops. Structural styles of these lower slope fields include compressional anticlines, turtle structures and sub-salt three-way dip closures against salt faces. Some of these reservoirs are highly compartmentalized by faulting. Older middle Miocene to Paleocene reservoirs in Gulf of Mexico are characterized by the following:

- Reservoirs are often at greater subsea depths: 20,000 to 30,000 ft.
- Reservoirs often have high pressure (>15,000 psi) and temperature (>180°F)
- Turbidite deposition was in coalescing basin floor fans, i.e. sheet sands
- Reservoirs are consolidated, resulting in lower rock compressibility
- Increased diagenesis in sands with volcaniclastic components results in cementation and reduced compressibility
- Paleocene reservoirs often have poorer porosity (<15%) and permeability (<30 mD)

In this study, the sample field located in the Gulf of Mexico. The example field has been developed with a semi-submersible production platform. Complex sea-floor topography plunges from 4,500 ft. to 7,000 ft. water depth at slopes up to 30 degrees. Several Miocene hydrocarbons bearing reservoirs are present over the structure at depths of 16,000 to 19,000 ft. subsea. A typical deep-water field water injection well is shown in **Figure 4-1**.

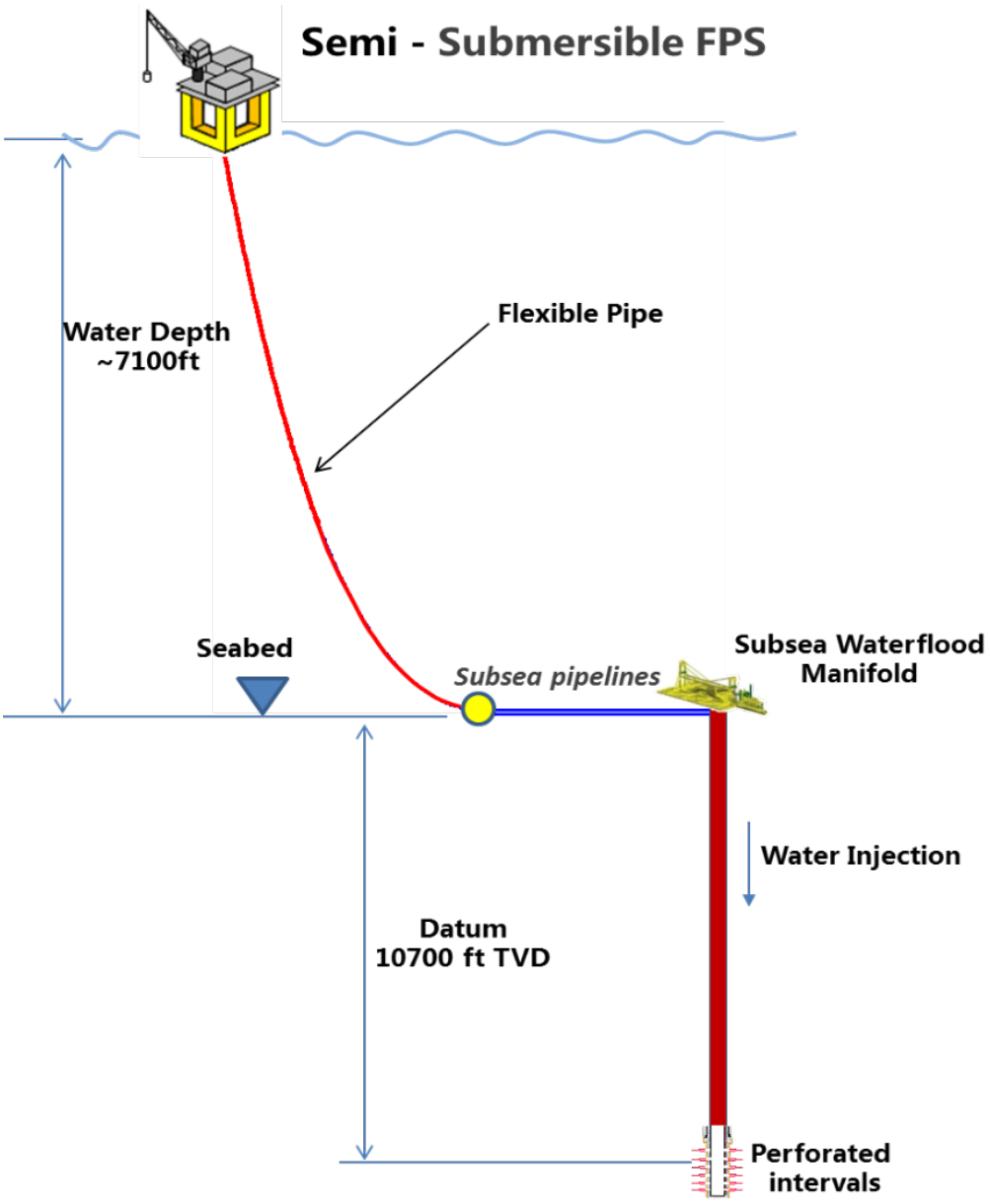

Figure 4-1 Sketch map of a deep-water field development (water injection well)

4.2 Case Studies

4.2.1 Example A

A summary of input data of Well A was shown in **Table 2** and **Table 3**, including reservoir properties, rock properties, injection properties, well data and tubing settings.

Table 2. Key reservoir and injection parameters for Well A		
Reservoir Parameters	**Unit**	**Value**
Original Reservoir Pressure	psi	9,500
Original Reservoir Temperature	°F	177
Current pressure at 0.47Re	psi	7,950
Drainage Radius	feet	1,500
Datum	ft TVD bwh	10,700
Rock Data		
Formation Gross Thickness	feet	100.0
Formation Net to Gross		0.60
Absolute Permeability	md	200.0
K_v/K_h		0.1000
End Point Water Relative Permeability		0.30
Young's Modulus	psi	1,481,481
Poisson Ratio		0.30
Coefficient of linear thermal expansion	1/°F	8.0E-06
Original Stress	psi	17,900
Injection Properties		
Thermoelastic shape factor		0.67
Injection water temperature	°F	70.0
Injection water total suspended solids	mg/l	2.0
Injection water oil-in-water	mg/l	2.0
Injection water total dissolved solids	%	5.0
Biot Factor		0.67
Well Data		
Well Deviation	degree	0.0
Well radius	feet	0.300
Well mechanical skin		0.0

Table 3. **Tubing settings for Well A**		
Tubing ID, in	Tubing Length, ft	Absolute Roughness
4.67	75	0.00024
5.25	11490	0.00024
3.88	130	0.0005

After applying the model described in Chapter 3, results of injection pressure versus water injection rate were presented in **Figure 4-2**. As in **Figure 4-2**, before the well was fractured, the increase of water injection rate results in the increase of both bottomhole injection pressure and wellhead injection pressure. When the well was fractured, BHIP and WHIP drop as water injection rate increases. The breakpoint in **Figure 4-2** indicates the existence of fracture, etc., when the water injection rate reaches 30,000 B/D and wellhead injection pressure reaches 15,300 psi, the well will be fractured. The slope before fracturing is steeper than the slope after fracturing, which also indicates the substantial increase of water injectivity. Moreover, it is noticed that after injection-induced fracturing occurred, the growth rate of well head pressure becomes larger than the growth rate of bottomhole pressure, and at some point, it will exceed bottomhole pressure. This phenomenon can be explained using **Eqn. 3-1**. Since the well head pressure is derived from BHP, because of the pressure drop due to friction along the tubing increases as the injection rate increasing, the difference between BHP and wellhead pressure will get smaller, which is showed in the graph. The physical meaning of this phenomenon is that at some point, the ability of a formation to receive injected fluid reaches its upper limit. In other words, the formation will not be fractured no matter what injection rate is.

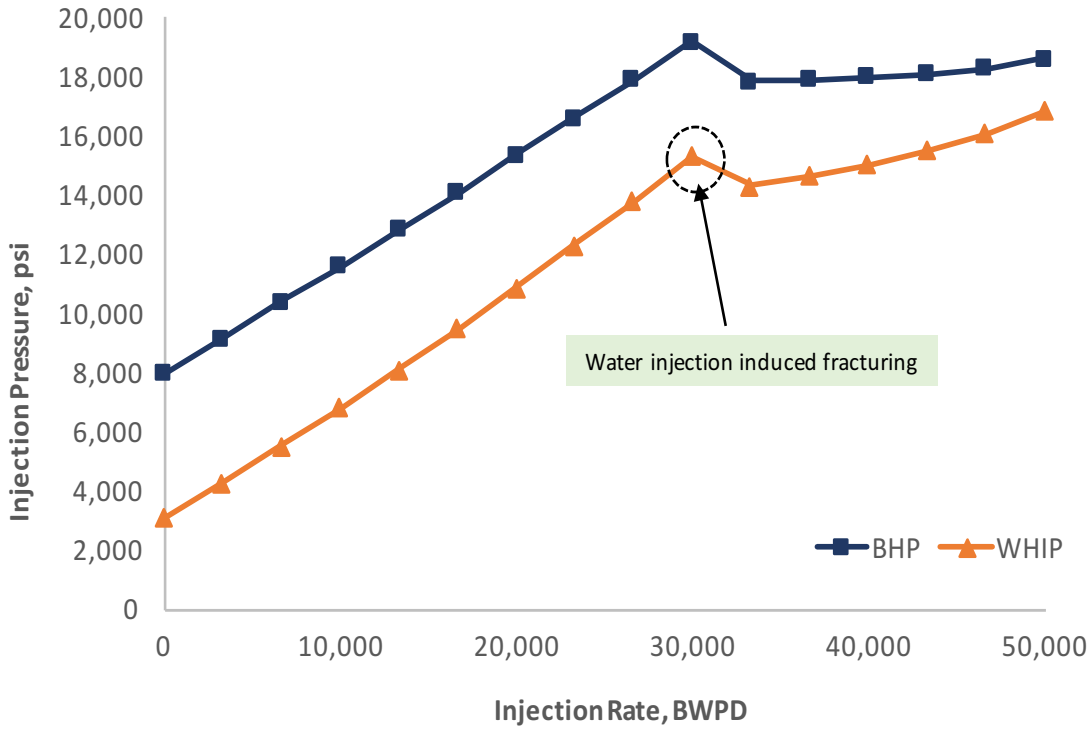

Figure 4-2 Well A bottomhole injection pressure and wellhead injection pressure versus water injection rate

4.2.2 Example B

In second case study, an injection well, Well B, will be discussed. The actual measured field data was shown in **Figure 4-3** and **Figure 4-4**. **Figure 4-3** shows the changes of water injection rate and bottomhole injection pressure over time. As shown in **Figure 4-3**, at point a, bottomhole pressure remains stable while water injection rate keeping increasing, which indicates the rock is fractured and propagates. However, the corresponding bottomhole pressure shall not be considered as fracturing pressure since the BHP is measured at downhole gauge. At point b, bottomhole pressure decreases while injection rate drops significantly. Comparing with point a, the injection rate is lower at point b while bottomhole pressure tends to be similar. The phenomenon may indicate the

collapse of fracture, which largely reduces the formation permeability. The fracturing can also be inferred in **Figure 4-4**. The two trend lines show in **Figure 4-4** illustrates the change of injectivity before and after fracturing. The injectivity, which is the reciprocal of the slope of the trendline, increased from 2.74 bbl/psi to 5.8 bbl/psi, which is caused by the injection-induced fracture. The point of intersection represents the occurrence of fracture, with corresponding water injection rate of 8243 B/D and downhole injection pressure of 10778 psi.

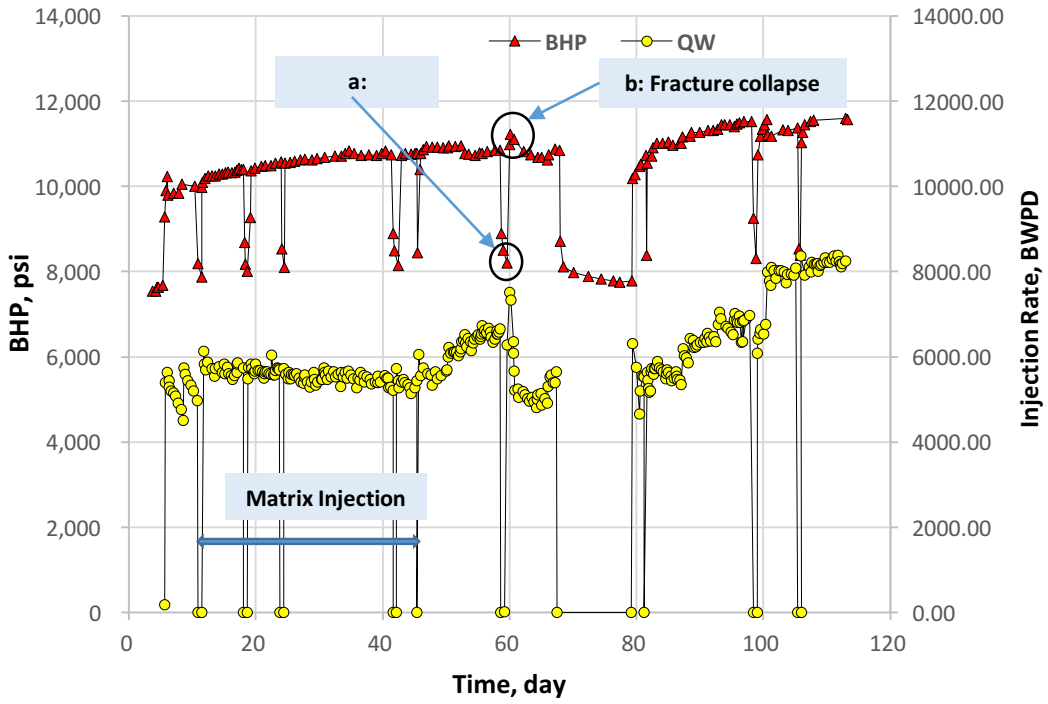

Figure 4-3 Measured flowing bottom hole pressure from permanent downhole pressure gauge and injection rate for Well B

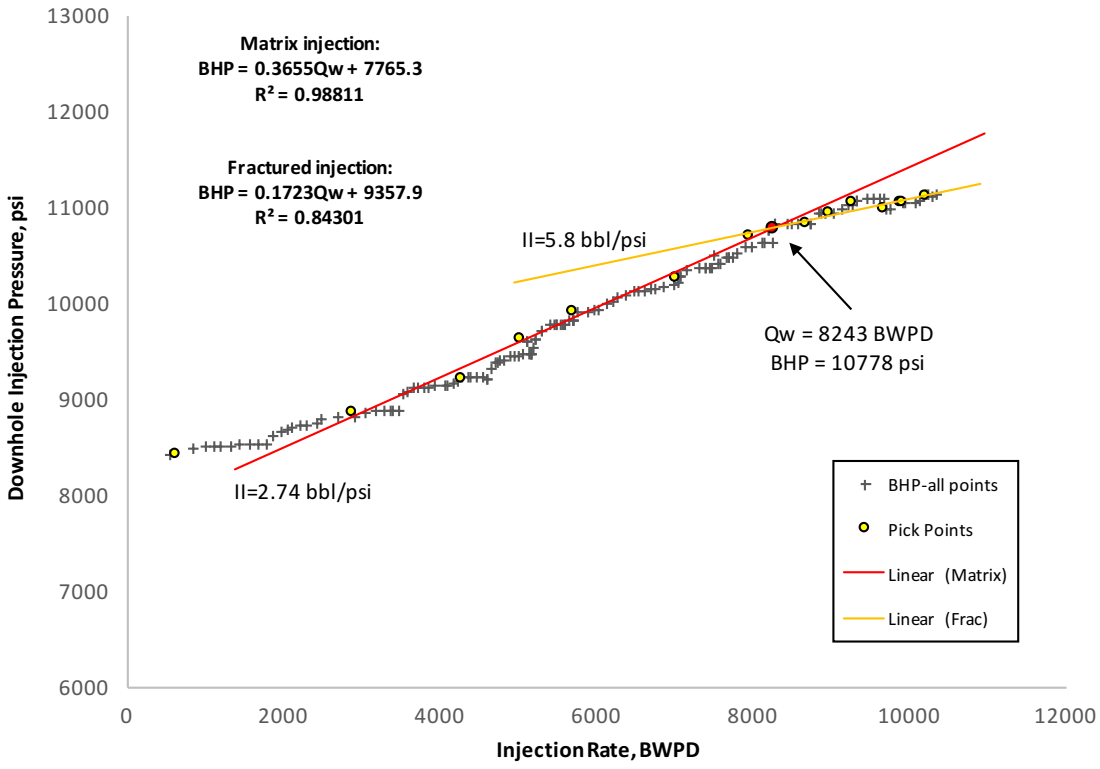

Figure 4-4 Step rate result for Well B, from which the change of slope indicates the change of injectivity

The measured data of Well B was then compared with calculated values using the program introduced in Chapter 3. From **Figure 4-5**, it is showed that the calculated bottomhole pressure before fracturing is basically consistent with the measured data of Well B. Also, the results are similar during the frac-packing completion (**Figure 4-6**). Therefore, it can be concluded that the model and program used in this study are highly reliable.

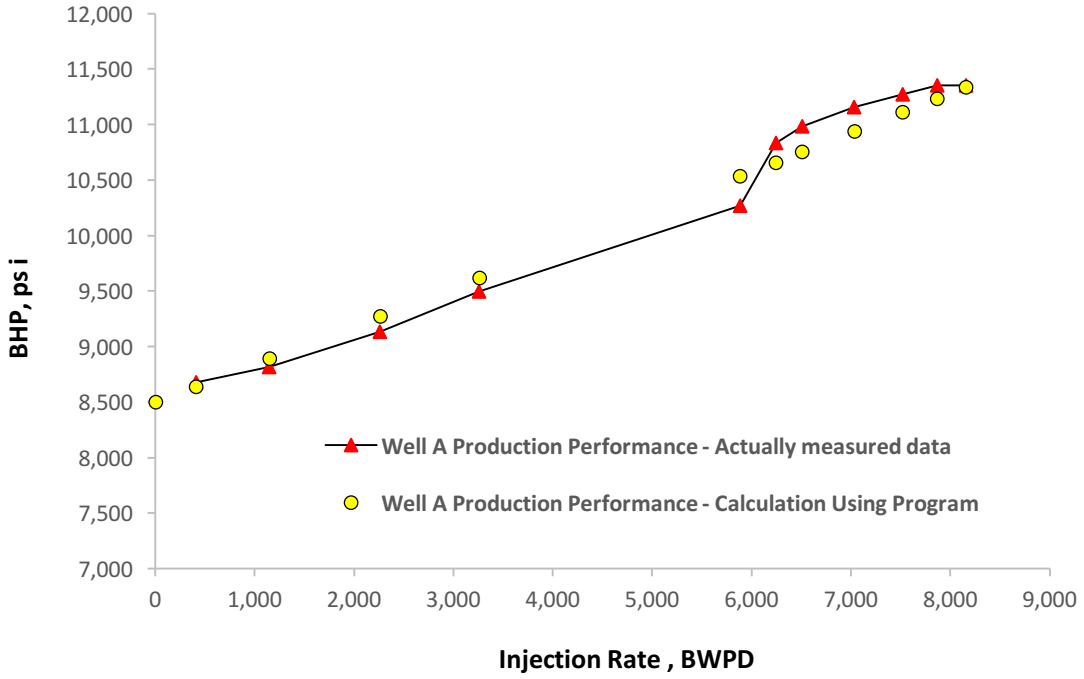

Figure 4-5 Comparison of measured and calculated values of Well B – production performance

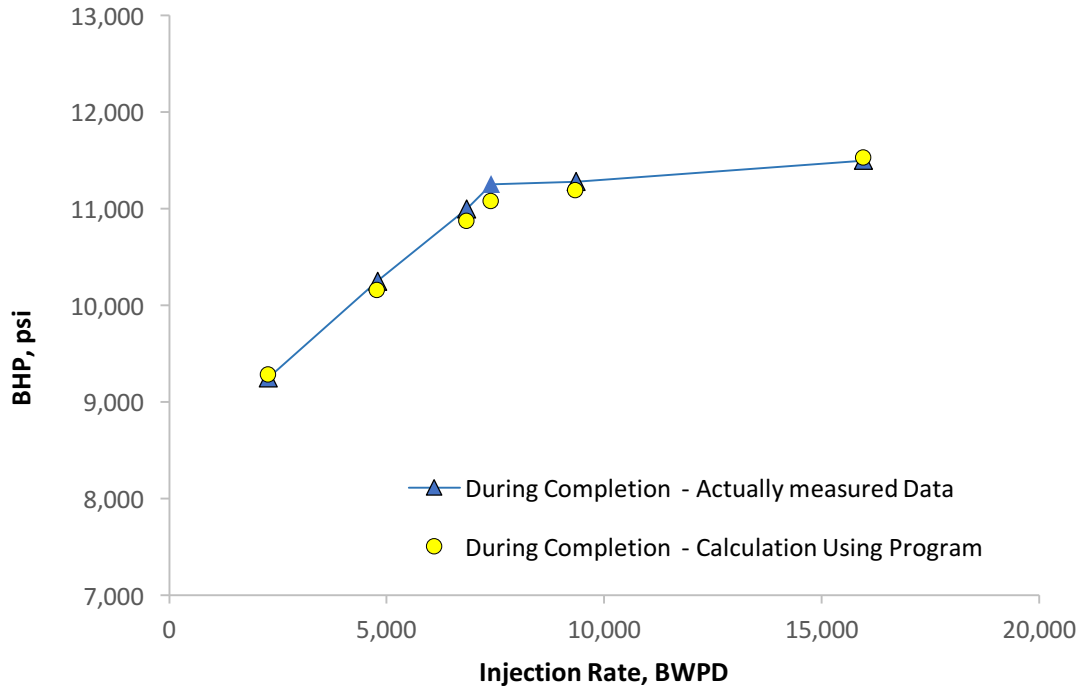

Figure 4-6 Comparison of calculated and measured value of Well B – during completion

4.3 Sensitivity Analysis

Sensitivity refers the degree to which model results are affected by changes in selected input parameters. In a typical fracturing pressure analysis, uncertainties exist in all factors introduced in Chapter 2, such as in-situ stresses, temperature, water quality and rock properties. A sensitivity analysis is necessary for fracturing pressure analysis to determine how uncertainties in the calculation of fracturing pressure are systematically apportioned to various input parameter factors. By investigating the relative sensitivity of the input parameters, the relative importance of parameters in the calculation process can be determined. When combined with uncertainty analysis, there can be more confidence in the predicted fracturing pressure.

A sensitivity analysis of various parameters was performed using these inputs, as shown in tornado charts **Figure 4-7**. The inputs can be generally classified in two categories, static inputs and dynamic inputs. Static inputs refer to parameters related to formation properties such as original stress, original reservoir pressure and temperature while dynamic inputs refer to parameters associated with water injection process, for example, injection water temperature, which can be controlled by operator. As shown in **Figure 4-7**, sensitivity result generated from influencing parameters indicates that the original stress is the most critical factor in the determination of fracturing pressure. Reservoir pressure and temperature also have greater influence on fracturing pressure. **Figure 4-7** also demonstrates whether those parameters have positive and negative influence on fracturing pressure. For example, the injection water temperature (assuming lower than reservoir temperature) would have direct influencing on fracturing pressure: the decrease of injection water temperature enlarges the temperature difference between injection

water and formation rocks, causing the reduction of fracturing pressure, which conforms the discussion in Chapter 2.

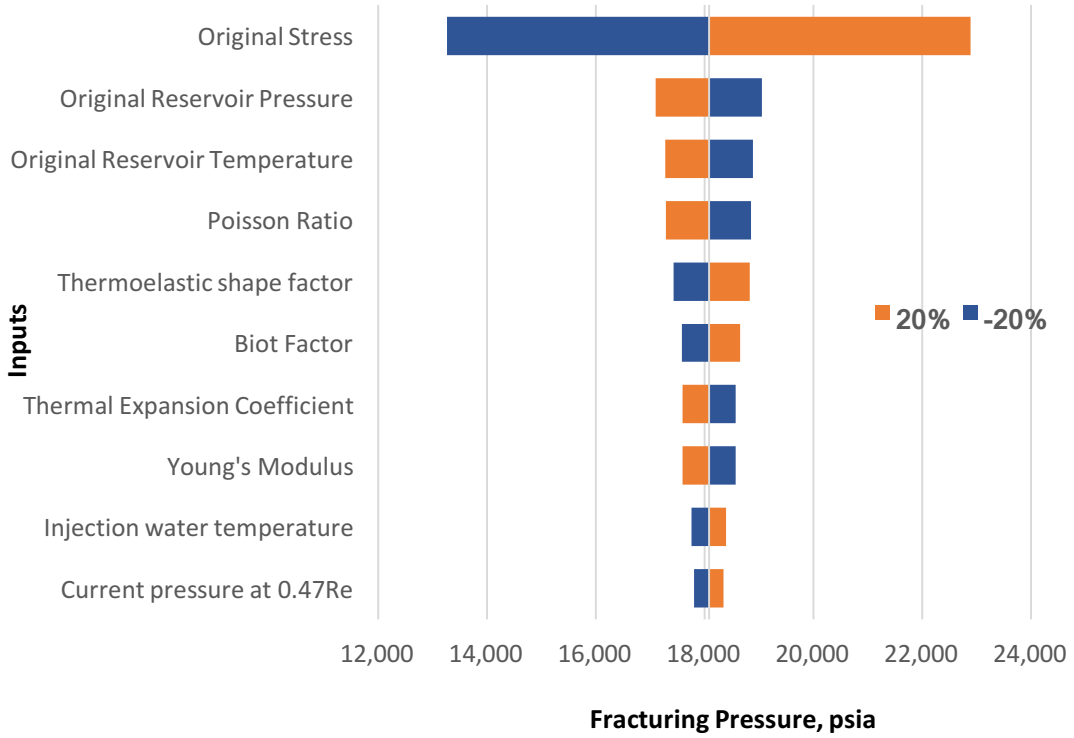

Figure 4-7 Tornado chart comparing the relative importance of inputs

As discussed earlier, water injectivity declines when large quantity of water is injected. Bottomhole pressure is sensitive to water quality, which is a factor that operators have control over. Therefore, in addition to fracturing pressure, another sensitivity analysis was performed to examine the relative importance of water quality on bottomhole pressure. It is shown in **Figure 4-8**, bottomhole pressure is most sensitive to suspended solids in injection water.

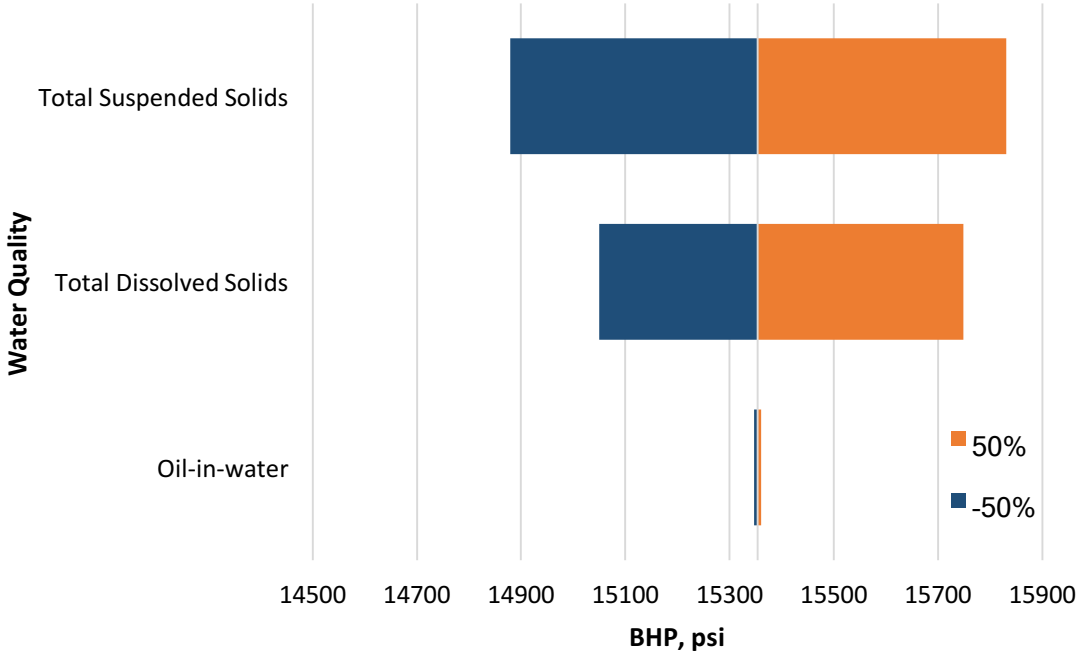

Figure 4-8 Tornado chart comparing the relative importance of water quality

4.4 Monte Carlo Analysis

A probabilistic analysis is necessary for fracture pressure analyses because geomechanical parameters are never known precisely, and because of an intrinsic uncertainty or error associated with each measurement. After the sensitivity analyses were performed to determine the relative effects of various factors on the fracture pressure, more attention was paid to those more sensitive parameters to better control the optimum mud-weight window. Less-sensitive parameters were filtered out to minimize the computational time. The terms P90, P50 and P10 are occasionally used to define confidence levels. Conceptually, the P10 is lowest value that the expert thinks that the uncertain variable could be. The P50 is the most likely value, while P90 is the highest estimate.

Uncertainties of each qualified input parameter were then quantified by simple probability distribution functions, such as uniform distribution, normal distribution, and triangle distribution functions. A Monte Carlo simulation process was performed based on the example Well A with input parameters as in **Table 4**; the result is shown in **Figure 4-9** and **Figure 4-10** with fracturing pressure of 17,068 psia at P10, 18,364 psia at P50 and 19,786 psia at P90. Therefore, in this case, P90 represents 90% of the calculated estimates (fracturing pressure) are lower than 19,786 psi. Among these three numbers, P10 and P90 show the range in the uncertainty of the estimate. P50 is usually considered as a best estimate since it is along with higher frequency in the frequency distribution. In other words, if the bottomhole injection pressure is even greater than P90, the formation will mostly likely be fractured.

Table 4. Input parameters for the example injection well (triangular distribution)

Parameters	Unit	Most likely	Min	Max
Original Reservoir Pressure	psi	9,500	9,000	9,500
Original Reservoir Temperature	°F	177	150	190
Current pressure at 0.47Re	psi	7,950	7,500	8,500
Poroelastic Shape Factor		0.67	0.60	0.70
Young's Modulus	psi	1.48E+06	1.48E+06	1.48E+06
Poisson Ratio		0.3	0.2	0.45
Coefficient of linear thermal expansion	1/°F	8.00E-06	7.5E-06	8.5E-06
Original Stress	psi	17,900	16,900	18,900
Injection water temperature	°F	70	55	120
Biot Factor		0.67	0.50	0.95

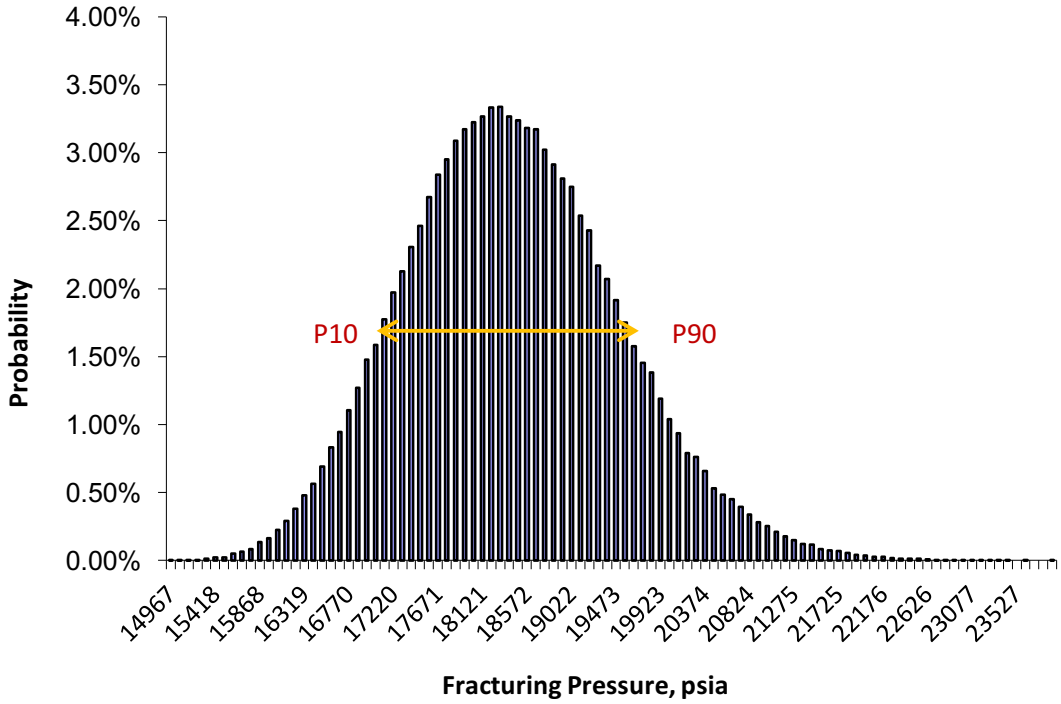

Figure 4-9 Probability density function of the fracturing pressure

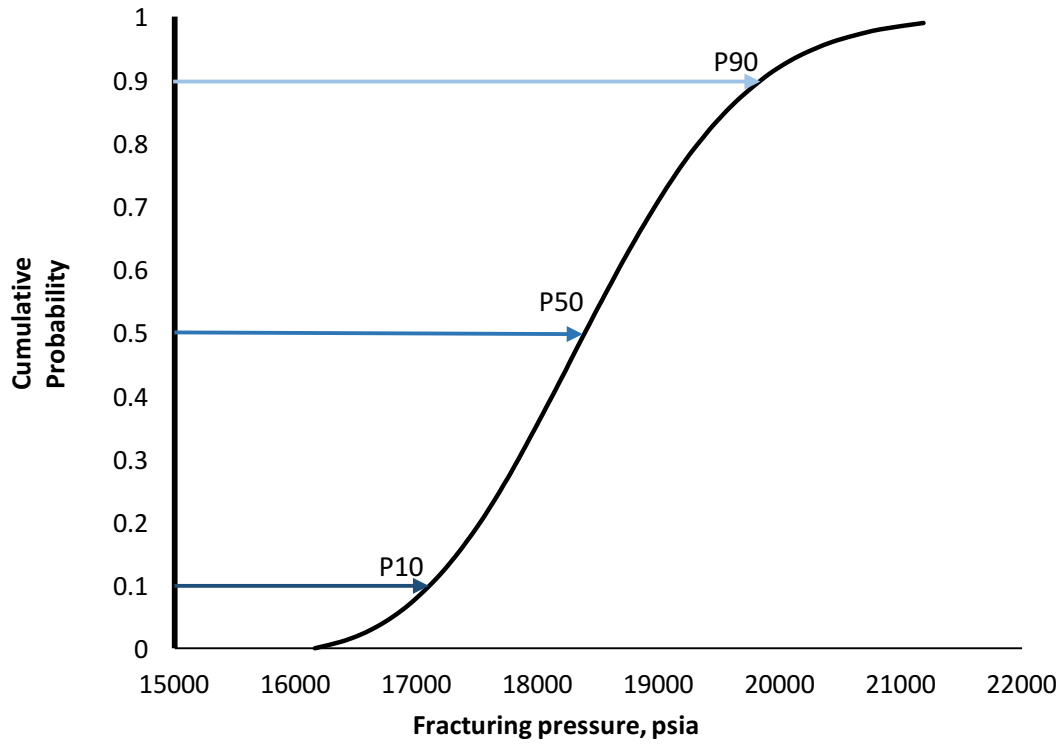

Figure 4-10 Cumulative distribution function of the fracturing pressure

Chapter 5: Conclusions and Recommended Future Works

This study explores many factors that affect the fracturing pressure of a formation, such as the in-situ stress, rock properties, and injection properties. The objective of the analysis was to quantify the range of subsurface uncertainty and to select deterministic models that represented the P10, P50, and P90 statistical subsurface realizations. To establish these deterministic models, we analyzed the sensitivity of the fracturing pressure to the subsurface uncertainties. In this study, methods for determining various input factors with the fracture pressure assessment by means of Monte Carlo simulations to understand the influence of various factors on fracture pressure were analyzed. The sensitivity analyses were performed to determine the relative influence of various factors on fracturing pressure. More attention was paid to the most-sensitive parameters to develop a better understanding of the controlling parameters in the determination of the fracturing pressure. As a result, less-sensitive parameters were filtered out to minimize the computational time. Case studies using the proposed methods are included to outline the workflow in the sensitivity investigation. After providing each input parameter with the designated functional distribution (e.g., normal, triangle, or uniform distribution), the Monte Carlo simulation was launched. The advantage of using the Monte Carlo simulation rests on the freedom to select the uncertainty range for each parameter and to indicate the confidence level of each input parameter. Consequently, the determined fracturing pressure can be more sensitive and realistic than those calculated from a deterministic model.

5.1 Conclusions

After extensive literature surveys on the controlling parameters for hydraulic fracturing models and influencing parameters, in this study, a stochastic procedure to determine the formation parting pressure for an injection is presented. Using the determined parting pressure, the procedure to determine the injection profile of the relationship between the pump pressure and injection rate are proposed. These procedures are validated against a deep-water injection well in GoM. From this study, the following conclusions can be drawn:

1) Formation parting pressure is affected by many parameters. For water injection scenario, the formation pore pressure, temperature changes in the near wellbore formation and injection pressure are critical.
2) Monte Carlo simulation of the parting pressure not only gives the ranges of possible parting pressure, but also give the probability of them. To minimize the range, uncertainties associated with geomechanics of rocks and injection conditions should be managed.
3) The determined profile between water injection pressure and flow rate can be a guideline for water injection practice. If the injection rate pressure exceeds the determined value or the injection rate is above the calculated rate, likely the injection induced fracture is going to be created.
4) In the injection process, it can be considered as a clear signal of fracturing formation when the injection rate increases, while the injection pressure decreases.

5.2 Recommended Future Works

Given the importance of knowing where the injection water goes in the reservoir management, the following surveillance and research are recommended.

1) Extend the model to multi-layer water injection.
2) Extend the model with pseudo-3D so that a more realistic model can be used to forecast the injectivity changes with injection pressure and rates.
3) Integrated water surveillance program for an asset should be established so that they can cross check each other to increase operator's confidence. The integrated surveillance technology includes Hall plot of water injection, distributed downhole temperature gauges, Capacitance-Resistance modeling, and reservoir simulation.

References

Agarwal, R. G., Gardner, D. C., Kleinsteiber, S. W., & Fussell, D. D. (1998). *Analyzing well production data using combined type curve and decline curve analysis concepts.* Paper presented at the SPE Annual Technical Conference and Exhibition.

An, F., & Cheng, Y. (2014). The effect of a tectonic stress field on coal and gas outbursts. *The Scientific World Journal, 2014*.

Bartlett, R. M., Singh, P. K., Howie, J. M., Humphrey, K., Kurtz, J. A., & Croft, M. D. (2010). *Unlocking Atlantis: An Integrated Approach to Reservoir Management of a Giant Subsalt Field.* Paper presented at the Offshore Technology Conference.

Biot, M. (1957). The elastic coeff cients of the theory of consolidation.

Charlez, P. A. (1997). Rock Mechanics: Petroleum Applications, vol. 2. *Editions Technip, Paris, France*.

Cinco-Ley, H. (1981). Transient pressure analysis for fractured wells. *Journal of petroleum technology, 33*(09), 1,749-741,766.

Crump, J., & Conway, M. (1988). Effects of perforation-entry friction on bottomhole treating analysis. *Journal of petroleum technology, 40*(08), 1,041-041,048.

Eaton, B. A. (1969). Fracture gradient prediction and its application in oilfield operations. *Journal of petroleum technology, 21*(10), 1,353-351,360.

Economides, M. J., Hill, A. D., Ehlig-Economides, C., & Zhu, D. (2012). *Petroleum production systems*: Pearson Education.

Fjar, E., Holt, R. M., Horsrud, P., Raaen, A. M., & Risnes, R. (2008). Petroleum Related Rock Mechanics (2nd Edition): Elsevier.

Geertsma, J., & De Klerk, F. (1969). A rapid method of predicting width and extent of hydraulically induced fractures. *Journal of petroleum technology, 21*(12), 1,571-571,581.

Gidley, J. L., Holditch, S. A., Nierode, D. E., & Jr., R. W. V. (1989). Recent advances in hydraulic fracturing. *SPE Monograph Series, 12*.

Harrison, E., Kieschnick Jr, W., & McGuire, W. (1954). The mechanics of fracture induction and extension.

Hettema, M., Bostrøm, B., & Lund, T. (2004). *Analysis of lost circulation during drilling in cooled formations.* Paper presented at the SPE Annual Technical Conference and Exhibition.

Hubbert, M. K., & Willis, D. (1957). Measurement of Hydraulic Fracturing. *Petroleum Transaction, Shell Development Co*.

Huffman Jr, A. C., Kinney, S. A., Biewick, L. R., Mitchell, H. R., & Gunther, G. L. Miocene of Southern Louisiana.

Khristianovic, S., & Zheltov, Y. (1955). *Formation of vertical fractures by means of highly viscous fluids.* Paper presented at the Proc. 4th world petroleum congress, Rome.

Koning, E. J. L. (1988). Waterflooding under fracturing conditions.

Liu, B., Dessenberger, R. B., McMillen, K., Lach, J. R., & Kelkar, M. G. (2008). *Water-Flooding Incremental Oil Recovery Study in Middle Miocene to Paleocene Reservoirs, Deep-Water Gulf of Mexico.* Paper presented at the SPE Asia Pacific Oil and Gas Conference and Exhibition.

Matthews, W., & Kelley, J. (1967). How to predict formation pressure and fracture gradient from electric and sonic logs. *Oil and Gas, 20*, 92-106.

Morgenstern, N. (1962). A relation between hydraulic fracture pressures and tectonic stresses. *Pure and Applied Geophysics, 52*(1), 104-114.

Nordgren, R. (1972). Propagation of a vertical hydraulic fracture. *Society of Petroleum Engineers Journal, 12*(04), 306-314.

Ovens, J., & Niko, H. (1993). *A New Model for Well Testing in Water Injection Wells Under Fracturing Conditions.* Paper presented at the SPE Annual Technical Conference and Exhibition.

Perkins, T., & Gonzalez, J. (1985). The effect of thermoelastic stresses on injection well fracturing. *Society of Petroleum Engineers Journal, 25*(01), 78-88.

Appendix A: Nomenclature

ρ	=	density, lbm/ft^3
β	=	Perkins and Gonzalez shape factor
α	=	Biot's poroelastic constant
ν	=	Poisson's ratio
σ	=	current stress, psi
ξ	=	Koning correction factor to account for the finite nature of the reservoir
θ	=	deviation of the wellbore from the vertical through the zone, degree
$\Delta\sigma_P$	=	induced poroelastic stress, psi
$\Delta\sigma_T$	=	induced thermoelastic stress, psi
σ_0	=	initial stress, psi
σ_e	=	current far-field stress, psi
σ_H	=	horizontal stress, psi
α_P	=	coefficient of pore pressure expansion
α_T	=	coefficient of thermal expansion
σ_{tect}	=	tectonic stress, psi
σ_v	=	vertical stress, psi
a_0	=	major semi-axis of an elliptical region
A_p	=	poroelastic coefficient

b_0	=	minor semi-axis of an elliptical region
BHP	=	bottomhole pressure at the formation face, psi
C_d	=	coefficient of discharge
C_{fD}	=	fracture dimensionless conductivity
D	=	diameter, inches
dL	=	length of the segment over which the pressure drop is calculated, ft
dP	=	pressure change, psi
E	=	Young's Modulus, psi
f_M	=	Moody friction factor
h_f	=	fracture height, ft
h_g	=	the gross thickness of the zone, ft
k	=	reservoir permeability, mD
k_f	=	fracture permeability, mD
k_h	=	horizontal permeability, mD
K_i	=	matrix stress coefficient
k_v	=	vertical permeability, mD
N_g	=	the ratio of the net to the gross thicknesses
N_p	=	number of perforations
N_{Re}	=	Reynolds number
OIW	=	oil-in-water, mL/g
p_0	=	the original reservoir pressure, psi
p_e	=	the current average reservoir pressure, psi

P_{frac}	=	the upper bound of fluid pressure in the bottomhole which would cause a fracture initiate from borehole wall
$P_{friction}$	=	frictional pressure drop through tubulars, completion and perforations, psi
$P_{hydrostatic}$	=	hydrostatic head due to the fluid column, psi
P_i	=	bottomhole injection pressure, psi
$P_{surface}$	=	surface pressure, psi
$P_{wellhead}$	=	wellhead injection pressure, psi
p_{wf}	=	bottomhole flowing pressure, psi
q	=	injection rate, BPM
Q_{total}	=	total flow rate, BPM
r_w	=	wellbore radius, ft
r_w'	=	effective wellbore radius, ft
s_f	=	skin due to fracture propagation
S_f	=	geometric shape factor
TDS	=	total dissolved solids, %
T_i	=	the injection water temperature, °F
TSS	=	total suspended solids, mL/g
v	=	velocity, ft/s
w	=	fracture width, ft
x_f	=	fracture half-length, ft
z	=	datum, ft
μ	=	viscosity, cp